PCCP

PERSPECTIVE

View Article Online
View Journal | View Issue

Cite this: *Phys. Chem. Chem. Phys.*, 2019, **21**, 20538

Received 29th July 2019,
Accepted 2nd September 2019

DOI: 10.1039/c9cp04222a

rsc.li/pccp

Structure of the aqueous electron†

John M. Herbert

Recently there has been a revival of interest in the basic structure of the aqueous or "hydrated" electron, e^-(aq). According to the conventional picture, this species occupies a cavity or excluded volume in the structure of liquid water, with a characteristic absorption spectrum ascribable to s → p excitations of a particle in a quasi-spherical box. This traditional picture has been questioned over the past few years, however, on the basis of a one-electron pseudopotential model that predicts a more delocalized spin density and no distinct cavity. This Perspective reviews the known experimental properties of e^-(aq) along with attempts to reproduce and understand them using both one-electron models and many-electron quantum chemistry calculations. The overwhelming weight of the evidence continues to support the conventional excluded-volume picture of the aqueous electron.

1 Introduction

1.1 Background

The aqueous or "hydrated" electron,[1–5] e^-(aq), is the primary reducing radical formed upon water radiolysis.[4–12] Its non-equilibrium precursor, the "pre-hydrated" electron, has frequently been implicated in radiation damage to DNA,[12–16] and while its role in that process is a matter of dispute,[17,18] the importance of e^-(aq) in the radiation chemistry of water is undeniable.[19] Fundamental interest in the aqueous electron has been revived in recent years by questions regarding the veracity of the canonical "cavity model" of e^-(aq).[20–24] According to this model, the thermalized electron occupies an excluded volume in the structure of liquid water (see Fig. 1), where it forms hydrogen bonds to somewhere between four and six water molecules,[25] coordinating to a single O–H moiety of each.[1,26–29]

A version of this model was postulated by Jortner and others in the earliest semicontinuum treatments of e^-(aq),[32–37] albeit without much convincing evidence at that time, but by the early 1980s this model had gained widespread acceptance.[37,38] This was due in large part to electron paramagnetic resonance (EPR) experiments by Kevan and co-workers,[26–28] which were interpreted as evidence of an unpaired electron in an octahedral coordination motif. Kevan's structural model is similar to the snapshots (from recent *ab initio* simulations[25,30,31]) that are depicted in Fig. 1, except perhaps for the precise coordination number. The instantaneous coordination number fluctuates in room-temperature simulations,[25] whereas Kevan's experiments were performed not in ambient water but in cold, highly alkaline aqueous glasses, *e.g.*, 10 M NaOH at T = 77 K.[27]

Starting in the mid-1980s, Rossky and co-workers pioneered simulations of e^-(aq) using electron-water pseudopotentials.[39–60] These simulations amount to what are essentially hybrid quantum mechanics/molecular mechanics (QM/MM) calculations with a one-electron QM region, described on a real-space grid for maximum flexibility in representing the structure of the (potentially delocalized) quantum-mechanical solute. Upon electron injection into neat liquid water, these models predict spontaneous electron localization accompanied by formation of an excluded volume, on a timescale of <1 ps. This is consistent with the electron localization timescale that is inferred from experiments.[61–71] Upon equilibration, the electron coordination motif predicted by these simulations is bond-oriented (O–H$\cdots e^-$) rather than dipole-oriented ($OH_2\cdots e^-$), consistent with the solvation motif inferred from various experiments.[27–29]

Rossky's results have since been replicated by several groups using more refined pseudopotential models,[72–74] sometimes in conjunction with many-electron quantum chemistry calculations.[75–79] Essentially the same picture emerges also from refined semicontinuum calculations,[80] and this picture is supported as well by *ab initio* molecular dynamics (MD) simulations under periodic boundary conditions, be they based on density functional theory (DFT),[25,81–83] correlated wave function theory,[31] or QM/MM simulations.[30,84,85] The various portraits of e^-(aq) that are shown in Fig. 1 demonstrate that all of these quantum chemistry-based simulations predict a localized, cavity-bound structure for the thermally-equilibrated hydrated electron at room temperature.

In constructing one's mental image of the cavity model, however, it is important to keep in mind that the solute is a quantum particle and is not strictly confined to the excluded-volume region. This feature has been present all along in

Department of Chemistry & Biochemistry, The Ohio State University, Columbus, OH, USA. E-mail: herbert@chemistry.ohio-state.edu

† Electronic supplementary information (ESI) available: Additional figures. See DOI: 10.1039/c9cp04222a

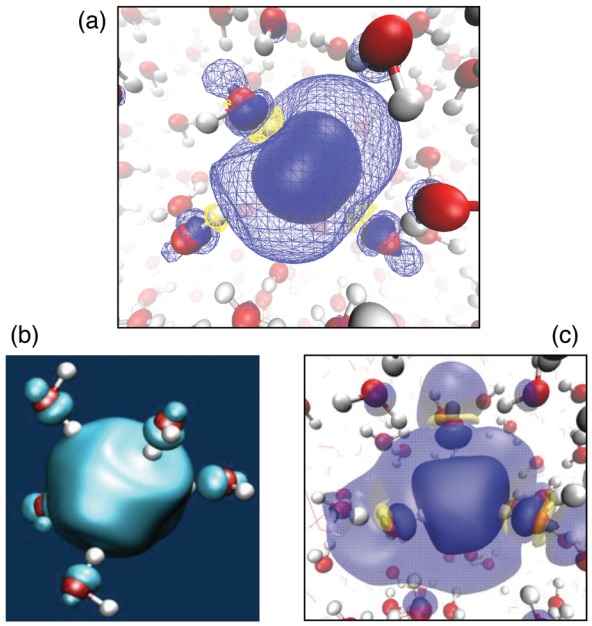

Fig. 1 Spin densities of the aqueous electron from *ab initio* calculations. (a) QM/MM simulation at the level of Hartree–Fock plus dispersion (HF+D3),[30] showing isoprobability contours that encapsulate 50% (opaque surface) and 85% (mesh surface) of $\rho_{spin}(\mathbf{r})$. (b) Periodic DFT simulation with a hybrid density functional,[25] showing a 60% isoprobability contour. For clarity only the first-shell water molecules are shown. (c) Periodic MP2 calculation,[31] illustrating 60% and 95% isoprobability contours. The regions in yellow that are visible in (a and c) indicate where $\rho_{spin}(\mathbf{r}) < 0$. These regions arise from the orthogonality requirement when the unpaired electron penetrates into frontier molecular orbitals of the water molecules. Panel (b) is reprinted from ref. 25, published by the Royal Society of Chemistry. Panel (c) is reprinted from ref. 31; copyright 2019 John Wiley & Sons.

theoretical simulations but sometimes overlooked, and it is possible to distort the visual image considerably by playing games with isosurface depictions of the wave function.[86–88] A variety of theoretical methods (including simulations with one-electron models,[73] static DFT calculations,[86,89,90] and *ab initio* MD simulations[84]) all concur that only 40–60% of the spin density,

$$\rho_{spin}(\mathbf{r}) = \rho_{\alpha}(\mathbf{r}) - \rho_{\beta}(\mathbf{r}), \quad (1)$$

is contained within the excluded volume. The tail of the e^-(aq) wave function penetrates two solvation shells beyond the cavity,[73,87] with bulk water structure recovered in the third solvation shell. This can be inferred by careful examination of the liquid structure (*e.g.*, number of hydrogen bonds per oxygen atom) and dynamics (autocorrelation function for H_2O librational dynamics), both of which return to bulk-like behavior in the third solvation shell of e^-(aq).[73] The small negative regions in $\rho_{spin}(\mathbf{r})$ that are evident in *ab initio* calculations (Fig. 1) result from the need to orthogonalize the singly-occupied molecular orbital (SOMO) with respect to the water MOs, resulting in a SOMO that contains nodes along the O–H bond axes of the hydroxyl moieties that coordinate directly to the electron. Even the very earliest Hartree–Fock studies of e^-(aq), including only a few water molecules around the electron, predicted that $\rho_{spin}(\mathbf{r}_H) < 0$ at the locations $\mathbf{r}_H$ of the hydrogen atoms nearest to the electron.[91–95]

The presence of tails in the aqueous electron's wave functions has led to suggestions that although the cavity model is partially correct, the true structure is somehow "complex".[84] The complexity is overstated, in this author's view. A two-parameter particle-in-a-box model, with a width (*i.e.*, cavity size) chosen to be comparable to the electron's radius of gyration (r_{gyr}, which can be inferred from the optical absorption spectrum[96–99]) and a well depth related to its vertical ionization energy (measurable using liquid microjet photoelectron spectroscopy[100–106]) is sufficient for a semiquantitative description of the spectroscopy of e^-(aq).[87,107] A simple quantum chemistry calculation that includes first-shell water molecules in a dielectric continuum also reproduces a variety of observables, qualitatively or semiquantitatively.[80] These models furnish a simple explanation for the main feature in the optical absorption spectrum,[75] which arises (according to the particle-in-a-box model) from three heterogeneously-broadened[108] s → p excitations,[42,73,75] as shown in Fig. 2. The long, Lorentzian "blue tail" in the absorption spectrum[99] (Fig. 2a) can also be rationalized within this picture, in terms of higher-lying bound- and quasi-continuum states.[75,87] Results from these simple models are borne out by detailed atomistic calculations.[25,73,75,76,85]

The cavity model emerges spontaneously in room-temperature simulations of e^-(aq) in bulk water, using both one-electron pseudopotentials[41,42,72–75] and many-electron quantum chemistry approaches.[25,30,31,81–85] Since 2010, however, this simple picture has been questioned by Schwartz and co-workers,[20,23,24,109–114] based on results from a one-electron pseudopotential model developed by Larsen, Glover, and Schwartz (LGS).[20] Simulations of e^-(aq) using the LGS model afford a very different picture in which no excluded volume is formed at all, and instead the spin density delocalizes over several water molecules with a slight enhancement of the water density near the centroid of the one-electron wave function. The essential structural differences between this prediction and the canonical cavity model are captured by Fig. 3, which depicts the one-electron wave function (*i.e.*, the spin density) obtained from a simulation with the LGS model, in comparison to that obtained using a cavity-forming pseudopotential model.

The difference between cavity and non-cavity models for e^-(aq) is also evident in plots of the $e^-\cdots$H and $e^-\cdots$O radial distribution functions (RDFs), $g(r)$, which are plotted in Fig. 4. Results from cavity-forming pseudopotential models developed by Schnitker and Rossky (SR),[40,41] and separately by Turi and Borgis (TB),[72,115] exhibit an unmistakable excluded volume, characterized by an effective radius r_0 such that $g(r) = 0$ for $r < r_0$. In contrast, RDFs obtained from the LGS model exhibit no such excluded volume. Although $g(r)$ does get smaller for this model as $r \to 0$ and the volume element shrinks (see Fig. 4b), depending on details of the averaging some simulations predict that $g(0) > 0$ for the LGS model.[76] (For an example, see Fig. S1 in the ESI.†)

Although various aspects of the LGS pseudopotential have been criticized,[21,22,76,116–118] this model does get the electron's radius of gyration approximately correct, predicting $r_{gyr} \equiv \langle r^2 \rangle^{1/2} \approx 2.6$ Å in comparison to the 2.44 Å that is inferred from the experimental absorption spectrum.[96–99] It also predicts

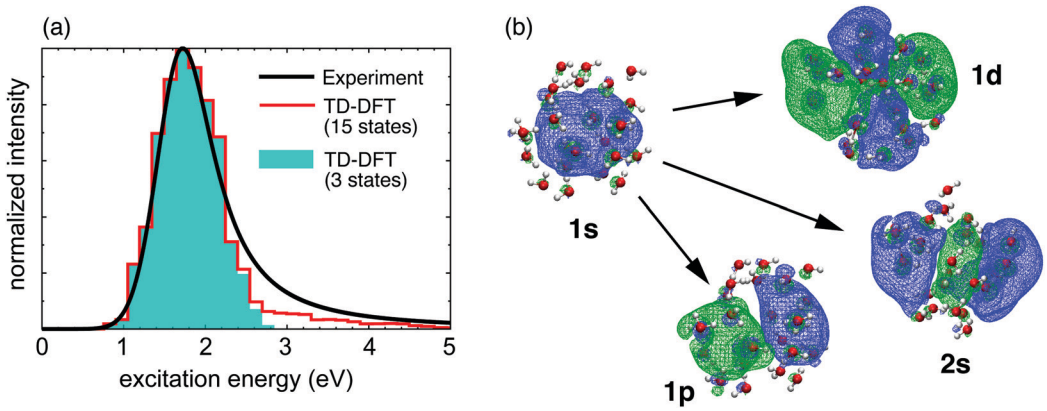

Fig. 2 (a) Experimental absorption spectrum of e^-(aq) along with time-dependent (TD-)B3LYP/6-31+G* calculations, averaged over many snapshots of the traditional cavity model.[76] (b) Representative TD-DFT natural transition orbitals from one particular snapshot, with quantum numbers suggestive of a "particle in a spherical box".[75] (Isosurfaces encapsulate 90% of the probability density, and classical water molecules from the QM/MM simulation are omitted for clarity.) The lowest three excited states are quasi-degenerate s → p transitions, and a TD-DFT calculation that is limited to only three excited states reproduces the main, Gaussian feature in the absorption spectrum. Adapted from ref. 75; copyright 2010 American Chemical Society.

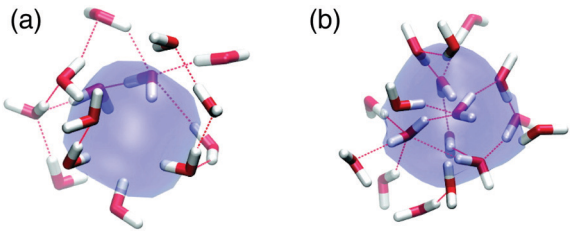

Fig. 3 Ground-state wave functions and nearby water molecules from simulations of e^-(aq) using (a) a cavity-forming pseudopotential model[73] and (b) the non-cavity-forming LGS model.[20] Both simulations were performed in bulk water but only water molecules within 4.5 Å of the electron's center of mass are shown. Isosurfaces encapsulate 70% of $|\psi(\mathbf{r})|^2$. Reprinted from ref. 76; copyright 2011 American Chemical Society.

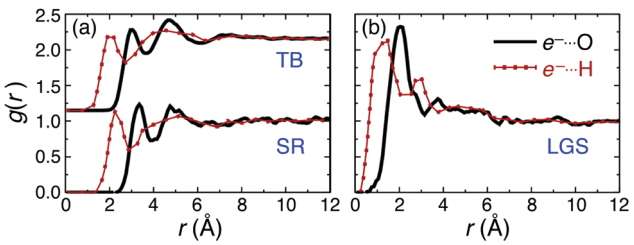

Fig. 4 Electron-oxygen and electron-hydrogen radial distribution functions obtained from (a) the cavity-forming Turi–Borgis[72,115] (TB) and Schnitker–Rossky[40,41] (SR) pseudopotential models of e^-(aq), and (b) the non-cavity model developed by Larsen, Glover, and Schwartz (LGS).[20] Adapted from ref. 109.

a reasonably accurate electronic absorption spectrum.[20] That said, it is not clear that the absorption maximum (E_{max} or λ_{max}) and the radius of gyration (r_{gyr}) are truly independent observables.[107] Moreover, it is difficult to reconcile the non-cavity prediction with the fact that all-electron quantum chemistry calculations consistently afford an excluded volume and a cavity-bound wave function.[25,30,31,81–85] The examples shown in Fig. 1 were taken from three different research groups using three different levels of theory: Hartree–Fock,[30] hybrid DFT,[25] and second-order Møller–Plesset perturbation theory (MP2).[31]

1.2 Aim and scope

The present article reviews the known experimental properties of the aqueous electron, with the goal of assessing the current state of simulations designed to connect these properties to an atomistic picture. Properties considered are listed in Table 1, and the rest of this work serves as a critique of how well these are (or are not) described by various theoretical models.

In addition to the SR, TB and LGS pseudopotential models that were introduced above, we also consider the "polarizable electron-water pseudopotential" (PEWP-2), a cavity-forming model developed by Jacobson and Herbert.[73] Like the TB and LGS models, PEWP-2 is based on the "static-exchange" approximation for the excess-electron wave function.[73,115,119,120] Unlike those models, PEWP-2 uses a polarizable force field[121] for the classical water molecules, and was originally developed in an effort to predict quantitative ionization energies for water cluster anions, which the model does successfully.[87,107] The self-consistent treatment of electron-water polarization also turns out to provide important corrections to the absorption spectrum of e^-(aq) in bulk water,[73,75,87,122] resolving long-standing difficulties in describing the complete spectral lineshape.[123] RDFs obtained from the PEWP-2 model are plotted alongside those from the TB and LGS models in Fig. S1 (ESI†). The cavity obtained from this model is slightly smaller and less structured as compared to that predicted by the TB model, but clearly evident nonetheless. Importantly, none of the pseudopotentials is specifically fit to any experimental data.[124]

In addition to these one-electron models, there is a category in Table 1 for many-electron quantum chemistry. For this, the present article draws upon DFT-based QM/MM simulations by Jungwirth and co-workers,[77,84,85] as well as several other *ab initio* simulations of e^-(aq) using periodic DFT.[25,81–83] Periodic MP2 simulations have also been reported recently,[31] as have Hartree–Fock QM/MM simulations.[30] All of these calculations

Table 1 Summary of e^-(aq) properties predicted by various theoretical approaches. The notation indicates whether a given model does (✔) or does not (✘) reproduce the property in question, or does so only qualitatively (≈). Question marks denote properties that have not been examined with the indicated model

Property	Many-electron quantum chemistry	One-electron pseudopotentials		
		Turi–Borgis (TB)	Jacobson–Herbert (PEWP-2)	Larsen–Glover–Schwartz (LGS)
Cavity forming?	Yes	Yes	Yes	No
Optical spectrum (E_{max} or λ_{max})	✔	✔	✔	≈
Radius of gyration (r_{gyr})	✔	✔	✔	✔
Coordination motif	✔	✔	✔	✘
Resonance Raman spectrum	≈	≈[a]	?	✘
Electron g-factor shift	≈	?	?	?
Hyperfine coupling constants[b]	✔	≈[a,c]	?	?
Diffusion constant	?	≈	≈	≈
Librational dynamics	?	✔	✔	?
Localization timescale	✔	✔	✔	✔
Vertical ionization energy	✔	✘	✔	✘
Hydration energy ($\Delta_{hyd}G^\circ$)	✔	?	?	?
Partial molar volume ($\bar{V}_{e^-}$)	≈	✔	≈	✘
T-Dependence of E_{max}	?	≈	?	≈
Excited-state (S_1) lifetime	?	✘	?	✘
T-Dependence of S_1 lifetime	?	✘	?	≈

[a] Requires many-electron quantum chemistry calculations, which are performed using liquid geometries obtained from simulations using the pseudopotential model. [b] Comparing experiments in 10 M NaOH at T = 77 K to simulations in neat liquid water at T = 298 K. [c] Computed using geometries from the Schnitker–Rossky pseudopotential.

afford an aqueous electron that occupies a cavity, as illustrated in Fig. 1.

2 Review of experimental data

Experimental properties of e^-(aq) are reviewed below in roughly the order that they are listed in Table 1.

2.1 Absorption spectrum

All of the models considered here reproduce the main part of the optical absorption spectrum, and therefore λ_{max} (or E_{max}), with a small shift (≈0.2 eV) to lower excitation energies in the case of the LGS model.[20,22] The observed "blue tail",[99] on the other hand, emerges from the pseudopotential models only upon a careful treatment of oscillator strengths and excited-state polarization.[73,75,87,122] In this sense, the tail can be said to be a many-electron property, and in fact it arises naturally from DFT calculations where the aforementioned polarization effects are inherent.[75–77] In contrast, these effects must be added explicitly to one-electron models, and for that reason a straightforward calculation of the excitation energies and oscillator strengths from any one-electron model should be expected to overestimate E_{max}, by perhaps 0.2–0.3 eV.[73,75,122] The SR and TB pseudopotential models do indeed overestimate E_{max} but the LGS model underestimates it, meaning that inclusion of self-consistent polarization would exacerbate rather than ameliorate the discrepancy between the LGS absorption spectrum and the experimental result.[22]

All-electron time-dependent (TD-)DFT calculations have been performed at liquid geometries obtained from the pseudopotential models, using a QM/MM protocol, and the results are consistent with the preceding discussion.[76] As shown in Fig. 5, the absorption spectrum computed at LGS geometries is significantly red-shifted relative to experiment while that computed at PEWP-2 geometries is blue-shifted by almost the same amount. The spectrum computed at TB geometries is nearly identical to the experimental result. It was later shown that the functional used in these calculations blue-shifts the spectrum relative to that obtained from an "optimally tuned" range-separated hybrid functional,[77] the latter of which offers a better description of excited states with charge-transfer character.[125] As such, the spectra in Fig. 5 likely underestimate the extent of the red-shift at LGS geometries while overestimating the blue-shift at PEWP-2 geometries.

The absorption spectrum of e^-(aq) at the air/water interface has also been a topic of interest.[77,78,110,126] The TB model predicts a red-shift in E_{max} of ≈0.5 eV for the interfacial electron as compared to the absorption spectrum of the bulk species

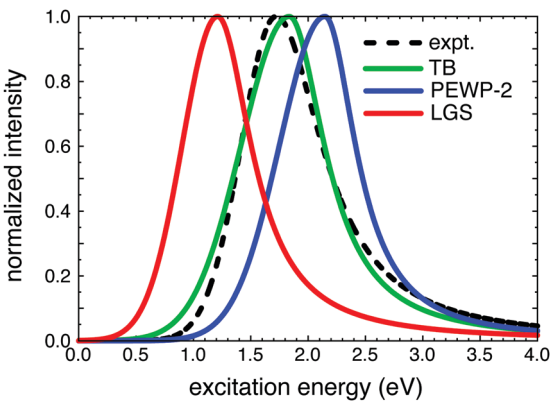

Fig. 5 Absorption spectra for e^-(aq) computed using TD-DFT with a range-separated hybrid functional.[76] The spectra are fits of TD-DFT excitation energies to a lineshape function, with liquid geometries obtained from the indicated pseudopotential models. Adapted from ref. 76; copyright 2011 American Chemical Society.

obtained using the same model.[110,126] In contrast, the interfacial absorption spectrum predicted by the LGS model is identical to its bulk spectrum.[110] No broad-band experimental absorption spectrum at the air/water interface is available, but QM/MM simulations combined with TD-DFT calculations do not find any evidence of a significant interfacial shift.[77] Furthermore, simulations using the TB model demonstrate that a hydrated electron initialized at the air/water interface rapidly internalizes into bulk water,[78,126] with spectroscopic observables that are nearly indistinguishable from those of the bulk species within a few picoseconds of dynamics at T = 298 K.[78]

At most, any interfacial red-shift appears to be a nonequilibrium property that would be challenging to measure in transient absorption spectroscopy. Single-wavelength transient absorption measurements have been carried out using surface-sensitive second harmonic generation (SHG), and these data suggest that hydrated electrons persist at the interface for at least 750 ps.[127] This is considerably longer than the internalization timescale observed in simulations,[78] although the "interfacial layer" (where inversion symmetry is sufficiently broken to yield an SHG signal) is perhaps 1–2 nm in depth,[127] which is more than enough for the interfacial spectrum to converge to the bulk spectrum.[78] It is likely that observables converge to bulk values well within the interfacial layer accessible to surface-sensitive spectroscopies.

2.2 Radius of gyration

Given the very different nature of the LGS wave function with respect to that predicted by any of the cavity-forming models, it is perhaps surprising that the spectral lineshapes are so similar. This is a unique feature of the relatively structureless wave function of the aqueous electron, or equivalently (in many-electron calculations) its SOMO, which in practice is essentially indistinguishable from the spin density. Simulations suggest that E_{max} for this peculiar system is governed by the size of the ground-state wave function and little else.[107] Quantifying the size of that wave function brings us to a second favorite point of identification for theoretical models of e^-(aq), namely, the electron's radius of gyration:

$$r_{gyr} = \left[\int (r^2 - \langle \mathbf{r} \rangle \cdot \langle \mathbf{r} \rangle) \rho_{spin}(\mathbf{r}) d\mathbf{r}\right]^{1/2}. \quad (2)$$

This quantity is experimentally accessible, within a one-electron approximation, from a moment analysis of hydrated electron's absorption spectrum.[96,99,128,129]

That being said, it is not clear that E_{max} and r_{gyr} are truly independent data points, as revealed by simulation data for $(H_2O)_n^-$ clusters obtained using the PEWP-2 pseudopotential model.[107] These data demonstrate that E_{max} tracks the radius of gyration extremely well, as does the vertical ionization energy (VIE). A plot of either quantity *versus* r_{gyr} (Fig. 6) reveals correlations that appear to vary as $1/r_{gyr}^2$. This is readily explained using the model of an electron in a spherical box, for which the lowest s → p transition energy is given by

$$\Delta E(r_{gyr}) = \frac{C}{r_{gyr}^2}. \quad (3)$$

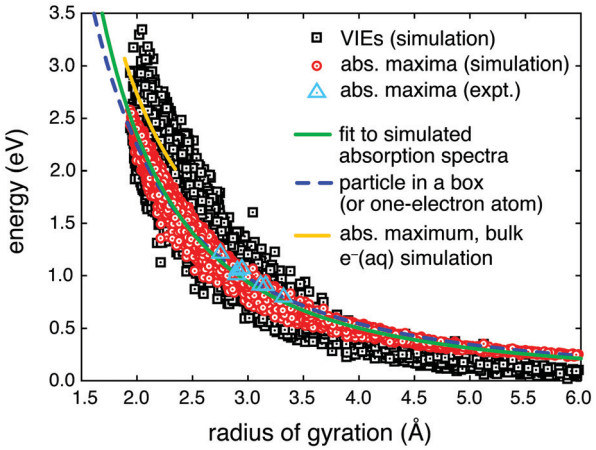

Fig. 6 Correlation between r_{gyr} and the VIE (black symbols), and between r_{gyr} and the electronic absorption maximum, E_{max} (red symbols), as measured for a variety of $(H_2O)_n^-$ clusters in simulations using the PEWP-2 pseudopotential model.[107] (These data include cluster sizes ranging from N = 20–200 simulated at either T = 100 K or 200 K, using a variety of initial conditions.) The dashed blue curve is the analytic result for a particle-in-a-box model whereas the green curve results from fitting the constant C in eqn (3) to the $E_{max}(r_{gyr})$ data obtained from the simulations. Experimental data for E_{max} (blue triangles) are obtained from the fit reported in ref. 99, which is based on cluster data originally reported in ref. 130. Simulation results for bulk e^-(aq) are from ref. 42 using the SR pseudopotential model, and are fit very well by the green curve when the latter is shifted upwards by 0.4 eV. Reprinted from ref. 107; copyright 2011 American Chemical Society.

(An analytic formula for the constant C is provided in ref. 107.) As shown in Fig. 6, the particle-in-a-box result is nearly identical to a curve in which the value of C in eqn (3) is simply fit to the data from atomistic simulations for clusters, not all of which even represent internalized states of the electron! Simulation data for e^-(aq) in bulk water, obtained using the SR pseudopotential model,[42] fall on essentially the same curve, as do experimental excitation energies for small $(H_2O)_n^-$ clusters.[99,130] Moreover, these correlations persist despite the fact that the simulation data in Fig. 6 sample a wide variety of electron solvation motifs and were obtained using different cluster sizes, temperatures, and initialization procedures.[107] Solvation motifs represented in these data include dipole-bound anions with very small VIEs, surface-bound isomers with larger VIEs, and also internalized isomers that are analogous to the cavity model of e^-(aq). VIE data obtained from *ab initio* MD simulations afford very similar VIE(r_{gyr}) curves for both water cluster anions[85] and for the hydrated electron in bulk water,[31,70,83,84] regardless of whether the quantum chemistry method is DFT or MP2.

The clear trend that emerges from all of these disparate sources of data allows us to predict with some confidence that any quasi-spherical probability distribution of roughly the right size (r_{gyr}) will produce a roughly correct excitation energy when a node is introduced into the wave function. In three-dimensional space, that node can be introduced in three independent ways, leading to a set of three s → p excitations that are broadened by fluctuations in the liquid environment.[108] In short, given r_{gyr}, one can predict E_{max} with reasonable fidelity either from a simple theoretical model such as the particle in a box

(or a hydrogenic ion model, which affords the same $1/r_{gyr}^2$ behavior for ΔE),[107] or from empirical fits to a wealth of existing simulation data.[70,84,107] The same is true for the VIE, although the VIE(r_{gyr}) distribution for $(H_2O)_n^-$ cluster anions is somewhat broader than the $E_{max}(r_{gyr})$ distribution. A detailed discussion of the VIE for the hydrated electron in bulk water be found in Section 2.8.

In view of the fact that all presently-debated theoretical models for e^-(aq) reproduce E_{max} reasonably well, it is not surprising that all of them reproduce r_{gyr} at least semiquantitatively. The radius of gyration predicted by the PEWP-2 model is a bit too small (calculated at 2.25 Å,[73] *versus* 2.44 Å inferred from experiment at 25 °C[99,131]), while the value r_{gyr} = 2.6 Å obtained from the LGS model is a bit too large,[20] and the TB value (2.42 Å) is spot-on.[72] Consistent with this line of argument is the fact that the LGS model slightly overestimates r_{gyr} while at the same time slightly red-shifting E_{max},[22] whereas the PEWP-2 model affords the opposite behavior: r_{gyr} is a bit smaller than the experimentally-inferred value and the spectrum is slightly blue-shifted.[73,75] In this author's view, these differences are insufficient to make meaningful distinctions amongst these models.

Considering many-electron *ab initio* simulations, the DFT-based QM/MM calculations reported by Jungwirth and co-workers afford r_{gyr} = 2.8 Å.[84] In comparison, $r_{gyr} \approx$ 2.2 Å for both periodic MP2 simulations,[31,131] as well as QM/MM simulations at the level of dispersion-corrected Hartree–Fock theory (HF+D3).[30] Both the HF+D3 and the MP2 simulations suffer from limited sampling (*e.g.*, a single 1 ps MP2 trajectory,[31] or a few 1 ps HF+D3 trajectories[30,118]), and there may be basis-set inadequacies as well, nevertheless the fact that these simulations predict a smaller value of r_{gyr} as compared to the DFT simulations is likely no accident. Rather, this probably reflects delocalization error in the DFT calculations, despite their use of an approximate self-interaction correction (SIC).[132] Consistent with this hypothesis is the fact that *ab initio* MD simulations using a hybrid functional (PBE + 40% exact exchange) afford a smaller radius of gyration, r_{gyr} = 2.49 ± 0.12 Å,[25] as compared to the semilocal BLYP(SIC)+D3 simulations by Jungwirth and co-workers.[84,85] The hybrid DFT value of r_{gyr} is in better agreement with experiment than is the BLYP(SIC)+D3 value.

2.3 Coordination motif

Despite significant differences in their predicted radii of gyration, QM/MM simulations at the HF+D3 level[30,118] and at the BLYP(SIC)+D3 level[84] afford remarkably consistent liquid structures for e^-(aq). This is apparent from a side-by-side comparison of RDFs, as shown in Fig. 7. (The same RDFs are directly overlaid in Fig. S2, ESI†) There is virtually no difference between the position, height, or width of the first peak in either the $e^-\cdots$H or the $e^-\cdots$O probability distribution. Differences are more noticeable in the second solvation shell, with the HF+D3 simulation resulting in a slightly more structured liquid, nevertheless these two rather different theories predict remarkably similar cavity structures. This, along with the fact that an excluded volume of similar size is stable at the MP2 level,[31] seems quite compelling. It suggests that there is little validity to the suggestion, put forward

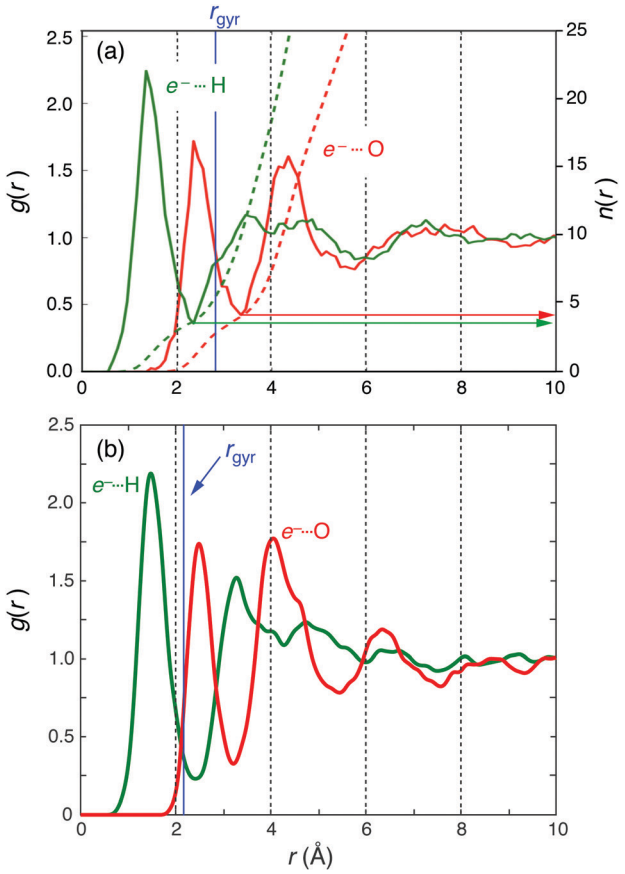

Fig. 7 Radial distribution functions from two different QM/MM simulations of e^-(aq): (a) BLYP(SIC)+D3,[84] and (b) HF+D3.[30] The dashed curves in (a) are the integrated coordination numbers $n(r)$ as defined in eqn (4), and should be read from the axis on the right. (Red and green arrows mark the first local minimum in either RDF.) The radius of gyration (r_{gyr}) is indicated for either simulation. Panel (a) is adapted from ref. 84; copyright 2012 American Chemical Society. Panel (b) is adapted from ref. 30; copyright 2019 American Institute of Physics.

by Glover and Schwartz,[111] that electron correlation effects have a tremendous impact on the structure of e^-(aq).[133] The liquid structure in the first solvation shell is apparently insensitive to the fact that the spin density is considerably larger at the BLYP(SIC)+D3 level (r_{gyr} = 2.8 Å) than at the HF+D3 level (r_{gyr} = 2.2 Å). This insensitivity does not seem consistent with the notion of a cavity that is on the verge of collapse but for subtleties in the potential, as Glover and Schwartz seem to imply.[111,133]

With the exception of the non-cavity LGS model, most other models predict that H_2O coordination to the unpaired electron occurs in a "bond-oriented" fashion (O–H$\cdots e^-$) involving a single hydroxyl moiety per water molecule. Bond-oriented solvation is predicted by one-electron models dating back to the pioneering simulations by Schnitker and Rossky[39,41,42] contemporaneous simulations by Berne and co-workers,[134,135] and the more recent TB and PEWP-2 simulations.[72,73] The same picture emerges from *ab initio* MD simulations based on many-electron quantum chemistry,[25,30,31,81,82,84,85] as evident from Fig. 1. In the few cases where dipole-oriented solvation ($OH_2\cdots e^-$) has been suggested in

quantum chemistry calculations on small $(H_2O)_n^-$ clusters, this has been shown to be a basis-set artifact.[88]

Experimentally, bond-oriented coordination has been inferred based on resonance Raman (RR) spectroscopy of e^-(aq) in isotopically-mixed water.[29] It is also the coordination motif that was proposed long ago by Kevan,[27,28] based on EPR experiments in alkaline glasses. The RR and EPR experiments are discussed in detail in Sections 2.4 and 2.5, respectively.

Quantum-chemical studies of e^-(aq) using small cluster models have sometimes fixated on determining its precise coordination number,[80,92,93] but *ab initio* simulations reveal that this number fluctuates in the room-temperature liquid.[25] Whereas Kevan proposed an octahedral model (*i.e.*, a coordination number n = 6) based on experiments performed at T = 77 K, simulations performed at T = 298 K using one-electron pseudopotentials afford coordination numbers $n \approx 4$ (TB and PEWP-2 models[73]) and $n \approx 5$ (SR model[41]). For the simulations, these are quantitative values obtained by integrating the function

$$n(r) = 4\pi \int_0^r (r')^2 g(r') \mathrm{d}r' \quad (4)$$

up to the first minimum in the electron-hydrogen RDF. The function $n(r)$ is plotted in Fig. 7a for the BLYP(SIC)+D3 simulations,[84] demonstrating that $n \approx 4$ for this simulation. Absent the empirical dispersion correction (+D3) and the empirical SIC, the BLYP functional affords a coordination number $n \approx 6$.[82]

Lastly on the topic of coordination motif, we note that the experimental RR spectrum of e^-(aq), which is discussed in detail in Section 2.4, is judged to be inconsistent with the "solvated solvent anion" model, H_2O^-(aq).[29] This has occasionally been floated as a possible microscopic picture of e^-(aq),[38,97,136–138] sometimes in the form [$HO^- \cdots H_3O$](aq),[136–138] although this model was always controversial,[137,138] and already in 1981 it was argued that the cavity model afforded a much better explanation for the available data.[38] In 2003, Tauber and Mathies[29] likewise rejected this model as inconsistent with the observation (based on RR spectroscopy in isotopically-mixed water) of one strong and one weak hydrogen bond per water molecule. These authors hold open the possibility that their data might be explained by a "solvated anion cluster" model,[29] or what Shkrob[89] has called the "multimer radical anion" model, wherein a small fraction of the unpaired electron is shared by several water molecules. This picture is not inconsistent with the cavity model, as the latter is certainly accompanied by $e^- \rightarrow \sigma^*_{OH}$ charge penetration into frontier MOs of water molecules in the first solvation shell.[139]

Another alternative picture is the "hydrated hydronium" or H_3O(aq) model,[140] which has been championed by Sobolewski and Domcke.[141–146] Within this model, which is supported by calculations in small clusters ranging up to $H_3O(H_2O)_9$,[141,142] the H_3O radical undergoes charge separation upon hydration such that this model resembles a contact ion pair, [$H_3O^+ \cdots e^-$](aq). To date, there are no theoretical calculations of H_3O(aq) in bulk water and therefore it cannot be said for certain whether the contact ion pair persists or whether the ions diffuse apart. It is therefore unclear whether the hydrated hydronium model actually differs in a meaningful way from the traditional cavity model. That said, the existence of a contact ion pair would be difficult to reconcile with conductivity data indicating that the ion mobility of e^-(aq) is more than twice that of the aqueous halides Cl^-(aq), Br^-(aq), and I^-(aq).[3] Setting aside this issue, which can only be resolved by examining H_3O in a truly aqueous environment, the RR spectra computed for small $(H_3O)(H_2O)_n$ clusters are not inconsistent with the experimental spectrum attributed to e^-(aq).[143,144] This is not altogether surprising, given that the e^-(aq) half of the ion pair bears much in common with the traditional cavity model of e^-(aq).

2.4 Resonance Raman (RR) spectrum

The RR spectrum of e^-(aq)[29,147–150] provides important information about the electron's coordination motif but is worth considering separately. By coupling s → p excitation of the electron with vibrational spectroscopy, it is possible to interrogate those water molecules that coordinate directly to the unpaired electron. The spectrum in the O–H stretching region is characterized by significant broadening and a frequency downshift of $\approx$200 cm^{-1} on the low-energy side,[29] relative to the normal Raman spectrum of neat liquid water. This is reminiscent of $\sim$300 cm^{-1} red-shifts that are observed in the O–H stretching frequencies of $(H_2O)_n^-$ cluster anions.[151–155] (See ref. 1 for a brief overview of the spectroscopy of water cluster anions.) The red-shifts observed in cluster spectroscopy have been studied with, and are reproducible by, DFT calculations,[139,152–154] a detailed analysis of which ascribes their origin to charge penetration of the unpaired electron into σ* orbitals of the O–H moieties.[139] This is just one example of a more general charge-penetration mechanism that explains O–H vibrational red-shifts in other anion-water complexes.[139,156,157] Sizable red-shifts have also been reported, computationally, in the RR spectra of small $H_3O(H_2O)_n$ clusters,[143,144] which exhibit a significant degree of $H_3O^+ \cdots e^-$ charge separation and thus manifest many of the spectroscopic features associated with the hydrated electron.[141–145]

Schwartz and co-workers have called the RR spectrum "the best experimental indicator of the hydrated electron's structure",[113] and have claimed that the O–H red-shifts are only reproduced by the LGS model and not by cavity models of e^-(aq).[24,109] In fact, Kevan-type octahedral $(H_2O)_6^-$ models of a cavity-bound electron, and analogous four-coordinate $(H_2O)_4^-$ models, both afford vibrational frequency red-shifts of 200–250 cm^{-1} according to DFT calculations.[80] Frequency shifts are not the same as RR intensity enhancements, although in view of the well-studied cluster spectroscopy cited above, it seems implausible that a cavity model of e^-(aq) would fail to manifest some kind of red-shift the RR spectrum. That is what is claimed by Schwartz and co-workers, however.[24,109]

A self-consistent calculation of the RR spectrum of e^-(aq) using a one-electron pseudopotential model is not straightforward because the classical water force field cannot be trusted to reproduce vibrational frequencies. (Moreover, such models lack the water orbitals necessary to describe $e^- \rightarrow \sigma^*_{OH}$ charge penetration.) To compute the RR spectrum, Schwartz and co-workers[24,109,113] rely on a "frequency map" technique in which the O–H stretching frequency ω is parameterized in

terms of the electric field strength F_{OH} along a given O–H bond vector:[158]

$$\omega(F_{OH}) = c_0 + c_1 F_{OH} + c_2 F_{OH}^2. \quad (5)$$

This empirical approach was developed by Skinner and co-workers for neat liquid water,[158–160] and works well for describing infrared and Raman lineshapes in pure liquid water and in ice.[158–161] However, eqn (5) was not reparameterized for use in e^-(aq), where the local electric field F_{OH} must include a contribution from the wave function that is likely quite different from anything in the training set of water clusters used to parameterize the original frequency map.[158]

This rather dubious methodology is unnecessary, as it is straightforward to compute a RR spectrum from first principles within the excited-state gradient approximation,[162–164] equivalent to the short-time approximation.[165,166] In this approach, the ratio of RR intensities for normal modes Q_j and Q_k is given by[162–164]

$$\frac{I_j}{I_k} = \frac{\omega_k(\partial\Omega/\partial Q_j)}{\omega_j(\partial\Omega/\partial Q_k)}, \quad (6)$$

where $\partial\Omega/\partial Q_k$ is the gradient of the electronic excitation energy Ω along the ground-state normal mode coordinate Q_k. Eqn (6) was used by Herbert and co-workers[118] to compute the RR spectrum of e^-(aq) within an "instantaneous normal modes" (INM) approach,[167] in which the Hessian is diagonalized (to obtain the frequencies ω_k) at unrelaxed snapshots taken from a QM/MM trajectory. The resulting RR spectrum, computed from unscaled harmonic frequencies, qualitatively reproduces the experimental spectrum over the entire infrared frequency range, as shown in Fig. 8a. These calculations were performed at the HF+D3/3-21++G* level, which affords a cavity-bound electron whose spin density is depicted in Fig. 1a.

The O–H stretching region is examined in detail in Fig. 8b, which includes the normal Raman spectrum of neat liquid water computed at the same level of theory. This comparison demonstrates a sizable red-shift of $\approx$300 cm^{-1} on the low-energy side of the RR spectrum of e^-(aq), consistent with experiment if somewhat exaggerated. This result stands in sharp contrast to the blue-shifted (and narrowed) RR spectrum for the cavity-bound electron that is reported by Schwartz and co-workers,[24,109] using the frequency-map approach.

INM calculations based on eqn (6) can also be performed using non-cavity liquid geometries obtained from a simulation with the LGS model, and those results are also shown in Fig. 8b. The spectrum computed at LGS geometries is down-shifted even further than the spectrum of the cavity-bound electron, although it difficult to ascribe quantitative significance to the numerical value of this shift due to the unavoidable mismatch between the method used to generate the trajectory and that used to compute vibrational frequencies. This mismatch is necessary because there is seemingly no many-electron model that affords a non-cavity electron. (Many quantum-chemical models do not even bind the excess electron at LGS geometries, as discussed in Section 2.8, and for that reason the non-cavity spectrum in Fig. 8b is computed at the PBE+D3 level.) In any case, the red-shift obtained from INM-RR calculations at LGS

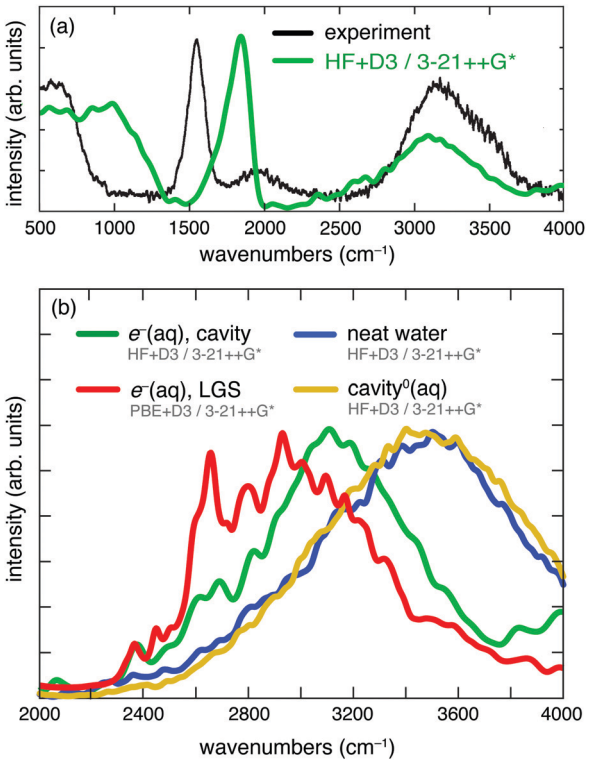

Fig. 8 Resonance Raman spectra of e^-(aq), and normal Raman spectra of liquid water, computed as ensemble averages of snapshots using an INM approach.[118] (a) Comparison of the experimental RR spectrum[29] to QM/MM calculations at the HF+D3/3-21++G* level,[118] for which a stable cavity (Fig. 1a) is maintained throughout the simulation. (b) Raman and RR spectra in the O–H stretching region, from various INM calculations. The green spectrum is the same HF+D3 calculation in both panels, whereas the red spectrum is a PBE+D3 calculation using non-cavity liquid structures obtained from LGS model. Also shown are the Raman spectrum of neat liquid water (in blue) and a "cavity^0(aq)" spectrum (tan color) that corresponds to an empty, charge-neutral cavity in liquid water. Adapted from ref. 118; copyright 2019 American Chemical Society.

geometries[118] is much larger than the shift of $\approx$50 cm^{-1} that is reported for the LGS model using the frequency-map approach.[109]

Computationally, one can remove the extra electron and thereby compute the normal Raman spectrum of an empty, charge-neutral cavity in liquid water, again within the INM approach. That spectrum, which is labeled "cavity^0(aq)" in Fig. 8b, is essentially indistinguishable from the Raman spectrum of neat liquid water computed at the same level of theory. This demonstrates that the sizable red-shift observed in the RR spectrum of e^-(aq) arises directly from the electron and not from changes that it induces in the liquid structure. This is consistent with the notion of $e^- \rightarrow \sigma^*_{OH}$ charge penetration as the origin of vibrational red-shifts.[139]

This charge-penetration effect seems to be rather non-specific and would likely manifest in any model of e^-(aq) that puts a semi-localized electron into liquid water. As such, the O–H red-shift alone cannot be used to discriminate between cavity and non-cavity models. More incisive are the RR spectra obtained in isotopically-mixed water.[29] Specifically, the spectrum of e^-(aq) in a 1:2:1 isotopic mixture of D_2O:DHO:H_2O gives rise to three

peaks in the bending region, two of which come from isotopically pure water, with a central peak arising from DHO. In the original experimental work,[29] this was interpreted as evidence of bond-oriented coordination leading to asymmetric solvation environments for the two hydroxyl moieties belonging to water molecules in the electron's first solvation shell. This feature was not addressed by Schwartz and co-workers, since there is no frequency map available for the bending region, but it can be addressed using quantum chemistry.

INM-RR spectra in D_2O, DHO, and H_2O are plotted in Fig. 9 for both cavity and non-cavity solvation motifs,[118] alongside the experimental spectrum in a 1 : 2 : 1 isotopic mixture.[29] In the experiment, two distinct bands emerge in the stretching region above 2000 cm^{-1}, and three bands are evident in the bending region. Bimodality in the stretching region is reproduced by cavity-forming QM/MM simulations but is absent in the INM-RR spectrum computed at non-cavity LGS geometries, which exhibit only a single band (albeit with some structure) above 2000 cm^{-1}. Fig. S3 (ESI†) shows a closer view of the bending region of the calculated spectra, demonstrating that cavity-forming HF+D3 simulations exhibit a doublet structure for the H–O–D bend that is not observed in spectra computed at LGS geometries.[118] It is difficult to rationalize why such a splitting should arise in the non-cavity case, given that the water molecules nearest to the spin density are fully embedded in that spin density, including both the O–H and the O–D oscillators in a DHO molecule.

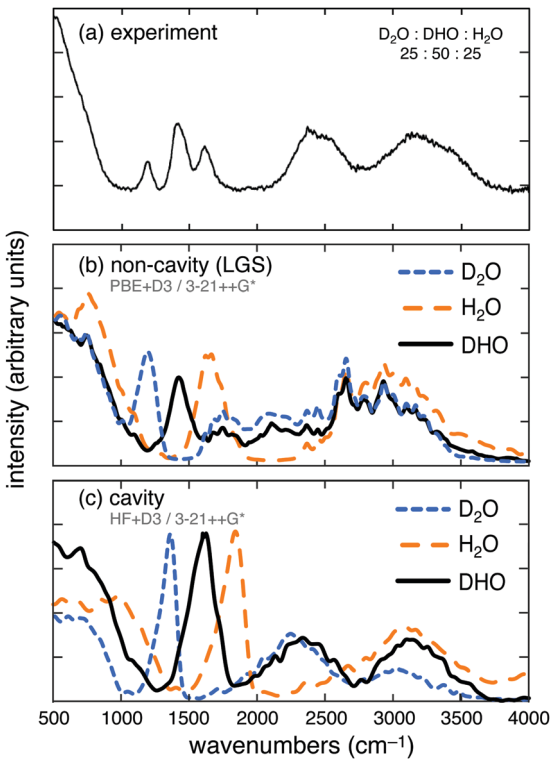

Fig. 9 Resonance Raman spectra of e^-(aq), including (a) the experimental spectrum[29] in a D_2O : DHO : H_2O mixture; (b) the INM spectra in D_2O, DHO and H_2O, computed at the PBE+D3 level using non-cavity liquid geometries obtained from a simulation using the LGS model;[118] and (c) the INM spectra computed for a cavity-bound electron at the HF+D3 level.[118] The data in (a) are reproduced from ref. 29. Panels (b) and (c) are adapted from ref. 118; copyright 2019 American Chemical Society.

In summary, the complete RR spectrum of e^-(aq), across the entire infrared frequency range, is reproduced qualitatively or even semi-quantitatively by low-level Hartree–Fock calculations that place the electron in a cavity. Additional features that arise upon isotopic substitution are also reproduced. The same cannot be said for spectra obtained from quantum chemistry calculations performed using non-cavity liquid structures obtained from the LGS model. Although the latter do afford a red-shift in the O–H stretching feature, they do not reproduce the additional structure that is observed in isotopically-mixed water.

2.5 EPR parameters

The microscopic picture of bond-oriented electron solvation was cemented by the work of Kevan,[27,28] at a time when some theoretical models were predicting dipole-oriented solvation instead.[37] This picture is based on ^1H and ^{17}O EPR and electron spin echo envelope modulation (ESEEM) experiments in alkaline glasses at 77 K.[26–28,168,169] These experiments were later reviewed by Shkrob,[89] who points out that the EPR spectra are structureless and can only provide constraints on the magnitude of the dipole coupling, not the coordination number directly, despite the fact that Kevan did infer a coordination number $n = 6$.[26–28] In light of ESEEM experiments subsequent to Kevan's,[170,171] Shkrob concludes that the interpretation of the EPR and ESEEM data in terms of a structural model is far from clear.[89] In particular, whereas the isotropic hyperfine coupling constant for the nearest-neighbor protons was originally determined to be $a_{iso}(^1H) = +2.1$ G by Kevan and co-workers,[168] a revised value $a_{iso}(^1H) = -0.92$ G was suggested by the later experiments.[170,171] (The difficulties in fitting Kevan's original data to a model Hamiltonian to extract a_{iso} are described by Shkrob.[89]) A negative value of $a_{iso}(^1H)$ is consistent with the existence of a node in the electron's wave function near the hydrogen nuclei.[80] Such a node is evident in *ab initio* simulations (see Fig. 1), where it arises from the requirement that the SOMO be orthogonal to the water MOs. In fact, such a node appears in essentially any many-electron quantum chemistry calculation in which a small number of water molecules is arranged around an excess electron in a bond-oriented fashion.[1,80,91–95] Negative spin densities predicted at the hydrogen nuclei were a source of great consternation in early Hartree–Fock calculations,[92–95] because it was assumed at the time that Kevan's experiments implied that $\rho_{spin}(\mathbf{r})$ should be positive at these nuclei.

The parameter a_{iso} originates in the Fermi contact interaction that depends on electron density at the nucleus, hence this and other EPR parameters (which are generally sensitive to electron penetration into frontier orbitals of the solvent molecules) are inaccessible to one-electron models of e^-(aq). Both isotropic and anisotropic hyperfine coupling constants can be computed using quantum chemistry, however. Results for cluster and semi-continuum models with a few bond-oriented water molecules are in reasonable agreement with experiment,[80,89] for both the ^1H and ^{17}O parameters. Not surprisingly, these parameters are

quite sensitive to electron-nucleus distance (*i.e.*, to cavity size),[80,89] and the isotropic constants are sensitive to the level of theory as well.[89] Given these uncertainties, the cluster calculations are unable to discriminate between four- and six-coordinate models of e^-(aq), although the anisotropic hyperfine coupling constants can be reproduced quantitatively for reasonable cavity sizes.[80] Semiquantitative agreement with experiment is also obtained for cluster models extracted from simulations using the one-electron SR model.[90] Given the very similar cavity structures predicted by the SR and TB models (see Fig. 4a), one anticipates that the TB model would afford similar agreement.

The electron *g*-factor for e^-(aq) has also been measured by EPR spectroscopy and is found to deviate significantly from its free-electron value, g_{free} = 2.00232. For e^-(aq), values g = 2.0006[172] and g = 2.0008[173] have been measured in ice at T = 77 K, with even smaller values obtained in liquid water: g = 2.0002 ± 0.0002,[174] g = 2.00033 ± 0.00003,[175] and g = 2.00047 ± 0.00007.[95] (As a point of calibration, these shifts are similar to those measured for NO_2 radical in the gas phase and for CO_2^- in matrix isolation spectroscopy.[95]) For e^-(aq), the experiments are mostly performed in highly alkaline solutions in order to suppress the concentration of electron-scavenging protons, but the experiments reported in ref. 95 are an exception; these were performed at neutral pH (and 22 °C) using only 0.05 M methanol to scavenge hydroxyl radicals.

The *g*-factor shift arises from spin–orbit (**L**·**S**) coupling, meaning that nonzero orbital angular momentum is required, and the observed shift is taken as evidence that the excess electron penetrates into oxygen 2p orbitals. DFT-based semicontinuum calculations using either four- or six-coordinate e^-(aq) structures afford shifts of 1200–1350 ppm,[80] *versus* the 1850–2120 ppm shifts obtained in the aforementioned experiments.[95,174,175] Both the *g*-shift and the hyperfine coupling constants depend sensitively on cavity size,[80,89] so it isn't clear that quantitative results for these observables should be expected from cluster or semicontinuum models, which lack an extended hydrogen-bond network to constrain the cavity. Overall, cluster models with bond-oriented coordination are in reasonable agreement with the known EPR spectroscopy of e^-(aq), as is the cavity-forming SR pseudopotential model. Hyperfine coupling constants have not been computed for LGS geometries so it is unclear whether non-cavity structures can reproduce the experimental observations or not.

EPR spectra of solvated electrons in ^{17}O-doped ice have been interpreted to suggest that ≈4% of the spin density resides in frontier orbitals of the water molecules.[27] (A nonzero value of a_{iso} for ^{17}O is also interpreted as evidence that the electron penetrates not just the oxygen 2p but also the 2s orbitals.[169]) With DFT calculations, one can attempt to quantify this electron penetration directly from the calculated spin density. To accomplish this, Uhlig *et al.*[84] use Voronoi polyhedra to partition the system into an excluded volume (cavity), along with volumes associated with each water molecule, and finally interstitial regions between the water molecules. They determined that ≈41% of the spin density resides in the cavity, with ≈24% overlapping the water molecules and the remaining 35% in the interstitial regions. As discussed in Section 2.2 and elsewhere,[31] it is likely that self-interaction error causes the BLYP(SIC) simulations of ref. 84 to overstate the extent of delocalization, despite the use of an empirical SIC. Nevertheless, it is clear that a significant fraction of the electron penetrates beyond the cavity. (Such penetration is also a feature of the cavity-forming pseudopotential models,[73,87] as discussed in Section 1.) The 24% of the spin density that is ascribed to the water molecules in the BLYP(SIC) calculations represents a sum over all of the molecules, in calculations that predict a coordination number $n \approx 4$, thus the total charge that is transferred to any one particular H_2O molecule is likely $<0.1e$. This is similar to the amount of $e^- \rightarrow \sigma^*_{OH}$ charge transfer that is estimated based on natural bond orbital analysis of water cluster anions.[139]

Although less sophisticated than the Voronoi analysis of ref. 84, Mulliken population analysis of small cluster models of e^-(aq) suggests that 10–20% of the spin density resides in frontier orbitals of the water molecules.[80,89,95] On this basis, Shkrob characterizes e^-(aq) as a "multimer radical anion", a model that he has put forward also for solvated electrons in acetonitrile,[176] in ammonia,[177] and in amines.[178] This is not inconsistent with the cavity model, and according to Shkrob the cavity arises due to the mutual repulsion of several nearby solvent molecules, each with a fractional negative charge. Problems with Mulliken populations aside, the present author considers this explanation unsatisfactory, at least in the case of the aqueous electron, in view of the >75% of the spin density that is clearly not tightly associated with the water molecules, as well as the ≈40% of the spin density that localizes in a very particular region of space, *i.e.*, in the cavity.[84]

2.6 Diffusion constant and librational dynamics

The diffusion constant for e^-(aq) at 25 °C has been determined *via* transient conductivity measurements, with reported values D = 0.475 ± 0.048[179] and 0.490 ± 0.003 Å^2 ps^{-1}.[180,181] This is about twice as large as water's self-diffusion constant at the same temperature,[182] and 2.6–3.0 times larger than diffusion constants measured for dilute solutions of NaCl(aq) and KCl(aq) at 25 °C.[183–186] The ion mobility of e^-(aq) is 60% that of H^+(aq) and approximately the same as that of OH^-(aq).[136] Given that both H^+(aq) and OH^-(aq) benefit from a Grotthuß proton-hopping mechanism,[187–189] whereas e^-(aq) does not,[44] one can surmise that diffusion of the hydrated electron is remarkably fast compared to other aqueous ions. At the same time, electron diffusion in water is several orders of magnitude slower than electronic diffusion in molten salts, as a consequence of the tight solvation sphere that localizes the aqueous electron.[190]

The bond-oriented coordination motif that was discussed in Section 2.3 plays a significant role in diffusion of the aqueous electron, which occurs *via* librational dynamics of the water molecules. This is a prediction from simulations using the SR and TB cavity-forming pseudopotential models.[44,191,192] (A mechanism along these lines has also been posited in experimental studies,[180] and simulations of the absorption

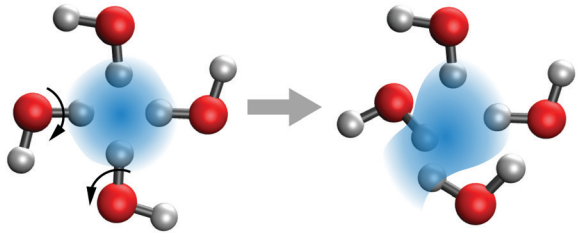

Fig. 10 Schematic depiction of the librationally-driven "oozing" that facilitates rapid diffusion of the aqueous electron.

lineshape with model Hamiltonians also suggest the importance of bending modes of the O–H moieties coordinated to the electron.[193,194]) As depicted schematically in Fig. 10, librational motion of one or more water molecules that is coordinated to the electron in a bond-oriented fashion serves to partially collapse the existing solvent cavity, while the same motion simultaneously opens up a neighboring void in the solvent. The hydrated electron thus oozes from one cavity into another, in a manner that does not require translational diffusion of any water molecule(s). This mechanism can explain the unusually fast diffusion of e^-(aq) without the need to invoke either a Grotthuß-style mechanism or long-range electron hopping.[44] Comparing e^-(aq) to Cl^-(aq), Br^-(aq), and I^-(aq), none of which benefits from Grotthuß-assisted diffusion, the ion mobility (conductance) is found to be 2.5–3.5 times larger for the hydrated electron than for the aqueous halides.[3,44,190] This can be attributed to the presence of librationally-assisted oozing in the case of e^-(aq).

Several calculations of the diffusion constant for e^-(aq) have been reported using one-electron pseudopotential models.[73,110,192] Before quoting the simulated results, it is worth noting that calculation of a diffusion constant from an atomistic simulation requires a long trajectory, since D is obtained by fitting to the asymptotic behavior of the mean displacement $\langle \|\mathbf{r}(t) - \mathbf{r}(0)\|^2 \rangle$. Values of D from relatively expensive QM/MM simulations therefore often come with sizable error bars due to the length of the trajectory. At T = 298 K, a value D = 0.6 Å^2 ps^{-1} is obtained using the TB model (with no error bars provided),[192] whereas PEWP-2 simulations at T = 300 K afford D = 0.79 ± 0.16 Å^2 ps^{-1}, with error bars that represent a 95% confidence interval.[73] While the latter value is a significant overestimate in percentage terms, the diffusion constant depends strongly on temperature and the experimental value increases from 0.49 to 0.52 Å^2 ps^{-1} just between T = 298 K and T = 300 K.[180] It was noted in ref. 73 that the simulated value of D at T = 300 K matches the experimental value measured at T = 317 K, whereas a simulated value D = 0.65 ± 0.18 Å^2 ps^{-1} is obtained from the PEWP-2 model at T = 282 K. These values can be characterized as being in semiquantitative agreement with experiment.

Schwartz and co-workers report a value $D \sim 0.5$ Å^2 ps^{-1} for the TB model at T = 298 K.[110] Curiously, they do not provide a numerical value for the LGS model, even though it is clear that the diffusive behavior was simulated in ref. 110 using both pseudopotential models. In ref. 23, however, they report that D = 0.20 ± 0.06 Å^2 ps^{-1} for the LGS model. This is considerably smaller than the experimental value, consistent with an overly attractive potential.

Simulations using the PEWP-2 model demonstrate that water molecules in the first solvation shell of e^-(aq) are subject to slower librational dynamics and larger-amplitude librational displacements as compared to water molecules in the first solvation shell around Br^-(aq).[73] Both solutes are coordinated in a bond-oriented fashion in cavities of roughly equal size, and the reason for the disparity in the dynamics is a softer restoring potential counteracting the librational displacements in the case of the delocalized solute e^-(aq). The restoring force is larger in Br^-(aq), where the solute is localized and thus the hydrogen bonds are highly directional. This provides additional evidence in support of the quantum-oozing model of e^-(aq) diffusion that is illustrated in Fig. 10.

2.7 Localization timescale

Related to the librational dynamics is the localization timescale for an electron that is initially generated in the conduction band of liquid water. In time-resolved experiments where an initially delocalized electron is generated at t = 0, the emergence of an absorption feature in the near-infrared is interpreted as the signature of electron localization. The consensus from a variety of experiments is that this process occurs on a timescale $\lesssim$0.5 ps,[61–71] with a thermalization rate constant $k = 1/\tau$ where τ = 1.1 ps,[103] and complete thermalization within 5–6 ps.[67,68] Not surprisingly, the same librational dynamics discussed in the context of ground-state e^-(aq) diffusion (Section 2.6) are thought to play a significant role in the relaxation dynamics of the electron following s → p excitation.[195–197]

The localization process can be simulated directly using the pseudopotential models, for which the wave function is represented on a real-space grid so that there is no problem with representing a completely delocalized state. Starting from a completely delocalized electron in a periodic simulation cell of equilibrated neutral water, the localization process is essentially complete within 0.5–1.0 ps, even at the air water interface, in simulations using the TB and PEWP-2 models.[78] The same behavior is observed in *ab initio* MD simulations at both the periodic MP2 level,[31] and also at the hybrid DFT level.[25] That said, the LGS wave function also localizes quickly,[22] so the localization timescale cannot be used to discriminate between structural models of e^-(aq). Detailed simulations of electron localization are discussed in more detail in Section 3.

2.8 Vertical ionization energy

Absolute energetics of e^-(aq) can be challenging to compute due to long-range polarization effects,[30,73,79] but these difficulties have been surmounted through a combination of large QM regions and continuum (Poisson equation) boundary conditions, which provide an exact treatment of charge penetration into the continuum region.[78,79] MP2 calculations with continuum boundary conditions, performed using liquid geometries obtained from the BLYP(SIC)+D3 simulations by Jungwirth and co-workers,[84,85] afford a VIE of 3.75 eV.[79] This agrees quantitatively with the most reliable values obtained from liquid microjet photoelectron spectroscopy,

which are 3.7 ± 0.1 eV[105] and 3.76 ± 0.05 eV[106] upon correction for inelastic scattering of the outgoing photoelectron.[198] The scattering correction accounts for the fact that liquid-phase photoelectron spectra are dependent on the wavelength of the photodetachment laser,[104–106] because the inelastic scattering cross section of the outgoing photoelectron is a function of its kinetic energy.[199] Application of this correction affords a "genuine binding energy" (as it is called in ref. 105) that is somewhat larger than the electron binding energies of 3.3–3.6 eV that were reported in earlier liquid microjet experiments.[100–104] The scattering-corrected VIE measured in large water clusters (~300 water molecules) is comparable to the scattering-corrected microjet result, at 3.55–3.85 eV.[200]

With a careful treatment of solvent polarization following ionization, the PEWP-2 model also affords a VIE of 3.7 eV.[73] This value was first reported in 2010, long before the publication of the "genuine" binding energy[105,106] and at a time when the available microjet measurements[100–103] and gas-phase cluster extrapolations[99] suggested a liquid-phase VIE of 3.3–3.4 eV. (Extrapolation based on experiments in much colder clusters afford a VIE that is a bit larger.[201]) Neither the TB nor the LGS model includes self-consistent polarization, so neither can be expected to reproduce the VIE. Nevertheless, a variety of computational methods afford VIEs in good agreement with the best available liquid-phase experiments, when applied to cavity-bound geometries of e^-(aq).[73,78,79]

The LGS model predicts a VIE of ≈5.5 eV[20,22] that is significantly larger than experiment, in part because this model lacks self-consistent electron-water polarization.[73,87] For comparison, the cavity-forming TB model also lacks self-consistent polarization and also overestimates the VIE, predicting 4.79 ± 0.09 eV.[73] (Finite-size effects have a significant influence on the VIE, in calculations performed under periodic boundary conditions, and smaller values of the TB model's VIE that are reported in some simulations are artifacts of these effects, as discussed in ref. 73.) A correction to the VIE to account for self-consistent electron-water polarization is estimated at −1.3 eV.[73] This correction brings the TB value into reasonable agreement with experiment but the LGS value remains at least 0.5 eV too large. Schwartz and co-workers[23,112] have argued that criticism of their model's VIE is unjustified, precisely because the model does not include proper electron-water polarization. However, this model contains essentially the same $V_{pol}(r) = -\alpha/r^4$ polarization potential that is used in the TB model.[124]

Setting aside the quantitative prediction of the VIE, some insight into these models can be gained at the level of Koopmans' theorem, which amounts to the approximation VIE ≈ $-\varepsilon_{SOMO}$. This approximation neglects orbital relaxation and electron correlation effects but includes polarization, and typical errors in Koopmans' theorem ionization energies are 0.5–1.0 eV.[88,202] Hartree–Fock QM/MM calculations afford $\varepsilon_{SOMO} \approx -3.0$ eV for cavity-bound structures. This is consistent, within the accuracy of the approximation, with an experimental VIE of 3.7–3.8 eV.[105,106,198] Fig. 11a plots the instantaneous values of $\varepsilon_{SOMO}(t)$ from a HF+D3 simulation; the average value is $\langle\varepsilon_{SOMO}\rangle = -2.96 \pm 0.42$ eV.[30] These simulations use a QM region with 24 water molecules, but tests with much larger QM regions suggest that ε_{SOMO} is converged.[118]

In contrast, when liquid snapshots are extracted from a non-cavity-forming simulation using the LGS model, but then a QM/MM calculation is performed using many-electron quantum chemistry, the Hartree–Fock SOMO is found to be unbound; see Fig. 11b.[118] In fact, even the earliest Hartree–Fock semi-continuum calculations,[91] using $(H_2O)_5^-$ as the atomistic region, found that fully hydrogen-bonded water networks do not bind an excess electron except for a weak continuum contribution. To obtain strong, short-range stabilization, dangling hydroxyl moieties were required.[91] These calculations are updated in Fig. 11b using liquid geometries extracted from the LGS model, which contain no dangling O–H groups (except transiently), since the hydrogen-bond network of water remains intact in this model. Despite the use of very large QM regions containing an average of 75 water molecules, the Hartree–Fock SOMO remains unbound and therefore does not localize, even in comparison to the LGS one-electron wave function.[118] It is not a bound state, but rather a frustrated (or discretized) continuum state,[88] trapped near the water molecules only by the finite extent of the atom-centered basis set.

A bound-state Kohn–Sham wave function can be obtained only by relying on artificial stabilization by self-interaction error, and Fig. 11b also shows the values of ε_{SOMO} obtained at LGS geometries using the PBE and PBE0 functionals.[118]

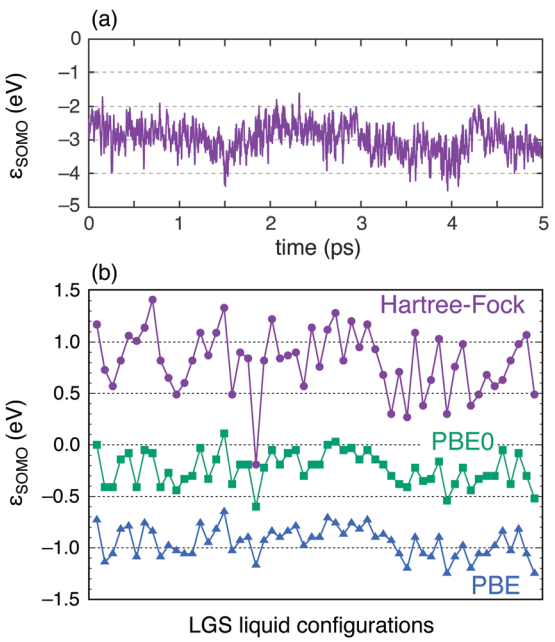

Fig. 11 (a) Fluctuations in $\varepsilon_{SOMO}(t)$ from an equilibrated, cavity-forming QM/MM simulation of e^-(aq) at the HF+D3/3-21++G* level.[30] The QM region in this simulation contains 24 water molecules. (b) Values of ε_{SOMO} obtained from QM/MM calculations, at liquid geometries taken from a simulation using the LGS model.[118] QM regions in these calculations contain an average of 75 water molecules, and calculations are performed at the HF+D3/6-31+G*, PBE0+D3/6-31+G*, and PBE+D3/3-21++G* levels of theory. Panel (b) is reprinted from ref. 118; copyright 2019 American Chemical Society.

The SOMO energy level is bound at the PBE0 level in most (though not all) of the snapshots, though it is more often unbound when smaller QM regions are used.[118] In contrast, the electron in a cavity forms a bound state when only first-shell water molecules are included. The PBE functional exhibits larger self-interaction error as compared to PBE0 and thereby stabilizes the SOMO level in smaller QM regions. Using large QM regions (as in the data shown in Fig. 11b), one obtains $\varepsilon_{SOMO} \approx -1.0$ eV for PBE+D3/3-21++G* calculations at LGS liquid geometries. Even this value seems too small to explain an experimental VIE of 3.7–3.8 eV, even in view of the limitations of Koopmans' theorem in DFT.[203,204] In short, the eigenvalue spectrum obtained from quantum chemistry calculations performed on e^-(aq) structures predicted by the LGS model is incompatible with the available photoelectron spectroscopy.

There has been significant interest also in the VIE of the hydrated electron at the air/water interface.[1,78] The TB model predicts a 0.5 eV reduction in the VIE at the air/water interface as compared to its value in bulk water, whereas the LGS model predicts no such shift.[110] Schwartz and co-workers suggest that the LGS model is therefore "more consistent" with the properties of the hydrated electron at the air/water interface.[112] They furthermore note that no feature at smaller binding energy has been observed experimentally, which is basically true. (There does exist one putative report of a smaller VIE for the hydrated electron at the air/water interface,[102] but the same feature is not observed in similar experiments,[103,205,206] nor is it evident in simulations or quantum chemistry calculations of the interfacial hydrated electron.[78,79] That said, VIEs of 1.4–2.0 eV have been measured for hydrated electrons on the surface of ice.[71,207]) MP2 calculations with nonequilibrium continuum boundary conditions, performed at BLYP(SIC)+D3 geometries, predict that the VIE is $\approx$0.4 eV smaller at the interface as compared to bulk water,[79] similar to the interfacial shift that is obtained from the TB model.[110]

That said, this point may be largely academic. Although the interfacial hydrated electron can be observed in time-resolved SHG experiments,[127] where it is generated within 1–2 nm of the air/water interface by photodetachment of I^-(aq), the barrier for surface $\rightarrow$ bulk internalization of e^-(aq) is $\approx k_BT$ according to free-energy simulations using the TB model.[110] Conventional MD simulations with the same model reveal that the interfacial electron persists for no more than a few picoseconds.[78] As discussed in Section 2.1, this is not inconsistent with the observation of e^-(aq) in surface-sensitive spectroscopy, but together with theoretical predictions for the interfacial absorption spectrum[77] it does suggest that the interfacial hydrated electron is spectroscopically very similar to the bulk species.

2.9 Free energy of hydration

On the subject of energetics, consider the molar hydration free energy of e^-(aq), $\Delta_{hyd}\bar{G}^\circ[e^-]$. Determination of this value from experiment requires an extra-thermodynamic assumption, since experimental measurements of equilibrium constants can at best determine $\Delta_{hyd}\bar{G}^\circ$ for ion pairs. As applied to water radiolysis, such measurements can be used, *e.g.*, to determine $\Delta\bar{G}^\circ$ for the process

$$H^+(g) + e^-(g) \rightarrow H^+(aq) + e^-(aq). \quad (7)$$

The free energy change for eqn (7) is determined to be $\Delta\bar{G}^\circ = -296.7 \pm 0.6$ kcal mol^{-1},[208] but in order to fix $\Delta_{hyd}\bar{G}^\circ[e^-]$ one must choose a value for $\Delta_{hyd}\bar{G}^\circ[H^+]$. Estimates of the latter range from -252.4 kcal mol^{-1} to -264.0 kcal mol^{-1},[209] which implies a range for $\Delta_{hyd}\bar{G}^\circ[e^-]$ from -44.3 to -32.7 kcal mol^{-1}. Kumar *et al.*[80] have recently revisited these data, including a careful evaluation of standard states and estimates for the value of $\Delta_{hyd}\bar{G}^\circ$ [H^+], and have concluded that the best estimate is $\Delta_{hyd}\bar{G}^\circ[e^-] = -36.3$ kcal mol^{-1}. This is not so different from earlier experimental estimates that put $\Delta_{hyd}\bar{G}^\circ = -38.6$ kcal mol^{-1},[210,211] or even the very early estimate $\Delta_{hyd}\bar{G}^\circ = -37.5$ kcal mol^{-1} by Jortner and Noyes.[34]

The value of $\Delta_{hyd}\bar{G}^\circ[e^-]$ has recently been computed from periodic DFT simulations using a hybrid functional.[25] The authors obtain a value $\mu_{hyd} = -1.28$ eV $= -29.5$ kcal mol^{-1} for what they call the "adiabatic redox level" of e^-(aq).[25] This value is subject to uncertainties arising from finite-size corrections to the energy levels of a charged system under periodic boundary conditions, as well as the need to align the absolute energy levels of e^-(aq) to those of neat liquid water.[25,212–215] Nevertheless, the agreement with experiment is reasonable, and the simulations are clearly cavity-forming, as seen in the snapshot shown in Fig. 1b.[25]

There have also been several attempts to compute $\Delta_{hyd}\bar{G}^\circ[e^-]$ based on cluster–continuum models of e^-(aq). These calculations afford values of -37.4 kcal mol^{-1},[216,217] and also -37.8 kcal mol^{-1} or -38.9 kcal mol^{-1},[80] depending on the particulars of the cluster model. Ostensibly, this is even better agreement with experiment as compared to the *ab initio* calculation quoted above, however the cluster–continuum calculations are not predictive. The cluster model must be manipulated in order to match experiment and there are issues associated with penetration of the diffusely-bound electron into the surrounding dielectric medium.[79] That these cluster–continuum calculations are able to match experiment so closely suggests that the value of $\Delta_{hyd}\bar{G}^\circ[e^-]$ is dominated by a combination of short-range solvation effects that can be captured by explicit consideration of $\approx$4 water molecules that are directly coordinated to the electron, along with long-range polarization that is describable by something along the lines of a Born ion model. The *ab initio* MD simulations in ref. 25, on the other hand, afford a first-principles prediction for $\Delta_{hyd}\bar{G}^\circ[e^-]$ that is clearly associated with an electron that carves out and occupies an excluded volume in the structure of liquid water. These calculations are free of both the "edge effects" associated with cluster models as well as uncertainties due to electron penetration into a dielectric continuum.

2.10 Partial molar volume

Another thermodynamic data point is the partial molar volume of the hydrated electron ($\bar{V}_{e^-}$), defined as the volume change upon addition of an electron to liquid water in the infinite-dilution limit. This quantity represents a particularly tangible probe of cavity *versus* non-cavity behavior. Schwartz and co-workers have

computed $\bar{V}_{e^-} = 31 \pm 12$ cm^3 mol^{-1} using the TB pseudopotential,[110] where the positive value is consistent with the intuitive notion that cavity formation should be accompanied by volume expansion. Similarly intuitive is the negative value that they compute using the LGS model, $\bar{V}_{e^-} = -116 \pm 27$ cm^3 mol^{-1}.[110]

Experimentally, Bartels and co-workers[218] have recently determined $\bar{V}_{e^-} = 26 \pm 6$ cm^3 mol^{-1} by measuring the pressure dependence of the equilibrium constant for the reaction

$$NH_4^+(aq) + e^-(aq) \leftrightharpoons NH_3(aq) + H(aq). \quad (8)$$

The value obtained in ref. 218 agrees quantitatively with time-resolved photoacoustic measurements of the volume change following photodetachment of $Fe(CN)_6^{4-}$(aq) or I^-(aq) to generate e^-(aq).[219,220] The value $\bar{V}_{e^-} = 26$ cm^3 mol^{-1} corresponds to a cavity radius of 2.2 Å, in line with electron-oxygen RDFs computed for the cavity-forming pseudopotential models; see Fig. 4a. Voronoi analysis of structures obtained from DFT simulations suggest a cavity radius of 1.8 Å even when $r_{gyr} = 2.49$ Å for the same simulation.[25] In contrast, it is difficult to reconcile any value $\bar{V}_{e^-} > 0$ with a non-cavity model that, in addition, predicts an enhancement of the liquid density in the vicinity of the electron's spin density.[20]

In defending the non-cavity model, Schwartz and co-workers have more than once falsely asserted that certain experiments suggest a value $\bar{V}_{e^-} < 0$.[23,110] As evidence, they cite an old pulse radiolysis study by Hentz and Brazier,[221] in which $\bar{V}_{e^-}$ is estimated from the pressure dependence of the forward rate coefficient for the reaction

$$H(aq) + OH^-(aq) \rightarrow e^-(aq) + H_2O\ (aq). \quad (9)$$

In fact, these measurements afford an activation volume ($\Delta\bar{V}^{\ddagger}$), which is an extra-thermodynamic quantity that is certainly not the same as a partial molar volume. Additional assumptions regarding the activated complex are required in order to obtain $\bar{V}_{e^-}$ from $\Delta\bar{V}^{\ddagger}$. As explained in ref. 76, the original claim by Larsen *et al.*[23] that $\bar{V}_{e^-} < 0$ appears to be based on a faulty reading of ref. 221, perhaps because a value $\Delta\bar{V}^{\ddagger} = -5.9$ cm^3 mol^{-1} for eqn (9) is quoted in the abstract of ref. 221 along with some comments about the partial molar volume of the hydrated electron. In both ref. 23 and again in ref. 110, Schwartz and co-workers appear to conflate $\Delta\bar{V}^{\ddagger}$ with $\bar{V}_{e^-}$, quoting -5.9 cm^3 mol^{-1} as the partial molar volume. (They finally concede, in ref. 112, that the experimental value of $\bar{V}_{e^-}$ is indeed positive.)

Upon careful reading of ref. 221 in its entirety, it becomes clear that conversion of the experimental data for $\Delta\bar{V}^{\ddagger}$ into an estimate for $\bar{V}_{e^-}$ results in ambiguity as to the sign of the latter. Eqn (4) in ref. 221 affords that work's main conclusion regarding the partial molar volume, which is that

$$-1.7 \leq \frac{\bar{V}_{e^-}}{\text{cm}^3\ \text{mol}^{-1}} \leq 2.7. \quad (10)$$

Making an estimate of the effects of electrostriction, Hentz and Brazier[221] go on to conclude that the limits established by eqn (10) are consistent with an electron in a spherical volume of 1–6 cm^3 mol^{-1}, corresponding to a cavity radius of 0.7–1.3 Å.

Actually, Hentz and co-workers carried out a whole series of pulse radiolysis experiments of this type,[221–226] measuring the pressure dependence of various rate constants to obtain $\Delta\bar{V}^{\ddagger}$ for reactions involving e^-(aq). Only in the earliest of these experiments do Hentz *et al.* ever put forward a value $\bar{V}_{e^-} < 0$,[222] and then only cautiously, with significant caveats. Even in that case, they conclude that upon consideration of the effects of electrostriction, their data are not inconsistent with formation of a small cavity.[222] In subsequent work, Hentz *et al.* would conclude that $\bar{V}_{e^-}$ is likely small but positive, with various estimates of the cavity volume, *e.g.*, 3–14 cm^3 mol^{-1},[224] 1–6 cm^3 mol^{-1},[221] 3 cm^3 mol^{-1},[225] and 10 cm^3 mol^{-1}.[226]

Schwartz and co-workers characterize this uncertainty as "discrepancy as to what the experimental molar solvation volume… actually should be".[110] This feels, to the present author, like obfuscation. The older estimates by Hentz and co-workers are certainly smaller than more recent measurements,[218–220] but when viewed collectively, even the older measurements suggest $\bar{V}_{e^-} > 0$. In any case, the most recent measurement by Bartels and co-workers[218] is based on the pressure dependence of an equilibrium constant, not a rate constant. Such a measurement does not require extra-thermodynamic assumptions to obtain $\bar{V}_{e^-}$, although assumptions are made regarding the partial molar volume of the hydrogen atom; see ref. 218 for details. It seems impossible to reconcile all of these measurements with the large, negative value of $\bar{V}_{e^-}$ that the LGS model predicts.

2.11 Temperature dependence of E_{max}

The temperature dependence of the hydrated electron's absorption spectrum is one of its most well-studied properties.[98,99,227–234] The spectrum red-shifts as a function of temperature (in both H_2O and D_2O, and also in alcohols[235]), but the effect is small, *e.g.*, 2.4–2.8 meV °C^{-1} in H_2O.[98,99,233] Schwartz and co-workers have simulated the temperature dependence of the absorption maximum, $E_{max}(T)$, with results from ref. 109 that are reproduced in Fig. 12a.

In support of the non-cavity LGS model, Casey *et al.*[109] note that simulations using the cavity-forming SR and TB models afford essentially no temperature dependence whatsoever for E_{max}, as is clear from Fig. 12a and from comparable simulations using the TB model that have been reported elsewhere.[236] In stark contrast, the LGS model predicts a sizable red-shift in E_{max} as the temperature increases, though the magnitude of the effect is grossly exaggerated with respect to experiment. Certainly from one point of view, the LGS model is the only one that predicts a qualitatively correct temperature dependence for E_{max}. (A few data points computed with the PEWP-2 model are shown in Fig. S4 (ESI†), and also fail to reproduce any temperature dependence.) A contrasting perspective is that, following a -0.25 eV shift in the TB excitation energies, which can be attributed to neglect of self-consistent electron-water polarization (as discussed in Section 2.1),[73,75,87,122] the TB prediction for $E_{max}(T)$ is actually quantitatively closer to experiment than is the LGS prediction, at every single temperature considered in Fig. 12a. This is despite the fact that the TB model predicts no T-dependent shift in E_{max} at all! Moreover, whereas the -0.25 eV shift in the TB results

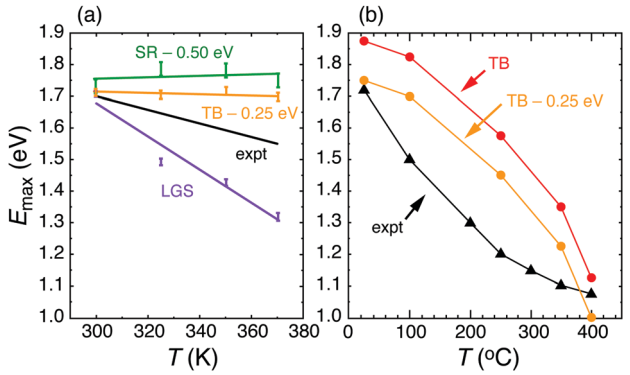

Fig. 12 Temperature dependence of the e^-(aq) absorption maximum. (a) Comparison of predictions from the TB, SR, and LGS pseudopotential models, for simulations at a fixed water density of 0.997 g cm^{-3}. The SR and TB values of E_{max} are shifted by −0.50 eV and −0.25 eV, respectively, as indicated. (b) Predictions from the TB model using liquid densities that correspond to the experimental density of neat liquid water at the indicated temperature. Note that the vertical scale is the same in both panels but that the data in (b) span a much broader range of temperatures, including supercritical data. Simulation data in (a) are from ref. 109 and experimental data are from ref. 234. Simulation data in (b) are from ref. 236 and experimental data are from ref. 237.

makes good physical sense, the fortuitously accurate s → p gap predicted by the LGS model is likely an artifact of this model's too-attractive behavior.[21,22,116,117] The TD-DFT optical spectrum at LGS geometries is strongly red-shifted (see Fig. 5), as discussed in Section 2.1.

Simulations used to obtain the data in Fig. 12a were performed using the canonical *NVT* ensemble at a single, fixed liquid density of 0.997 g cm^{-3} at each temperature.[109] These simulations (and others[236]) demonstrate that the cavity-forming TB and SR pseudopotential models exhibit no temperature effect on E_{max} for simulations at constant density. However, liquid water's density changes from 0.997 g cm^{-3} at 25 °C to 0.958 g cm^{-3} at 100 °C, an effect that is not taken into account in the aforementioned simulations. This reduction in the density at 100 °C is sufficient, in an *NVT* simulation, to produce a ∼0.1 eV red-shift in E_{max},[236] about half of the experimentally-observed shift over the same temperature range.

Nicolas *et al.*[236] have extended these simulations into the supercritical regime (Fig. 12b) in simulations that employ the experimental density of pure water at each temperature. Over the temperature range from 25–400 °C, corresponding to fluid densities ranging from 1.00–0.48 g cm^{-3}, they obtain a red-shift in E_{max} that is comparable in magnitude to the experimental result. On the basis of these simulations, it seems that the TB model does predict qualitatively correct behavior for $E_{max}(T)$, but that the magnitude of the observed effect is simply too small to be reliably simulated at subcritical temperatures. The pressure dependence of E_{max} has also been measured,[238,239] and the absorption spectrum is found to blue-shift with increasing pressure, consistent with a cavity that becomes smaller at higher pressure. This is likely the primary effect that is responsible for the relatively large *T*-dependent shifts that are determined by Nicolas *et al.*[236] when the temperature dependence of the density is taken into account.

It is worth noting that DFT-based *ab initio* MD simulations predict that a localized e^-(aq) wave function persists even in supercritical water,[81,82] although its coordination number is reduced.[82] Even at supercritical water densities as low as 0.32 g cm^{-3}, where the coordination number is reduced to $n \approx 2$, an excluded volume is still evident from the RDFs.[82] In fact, the size of this excluded volume is not significantly different from that obtained for comparable simulations in ambient water.[82]

Bartels and co-workers[234] have measured the e^-(aq) absorption spectrum in supercooled liquid water, where a red-shift of 2.2 meV $°C^{-1}$ persists down to at least −18 °C. As a consequence of water's density anomaly, their data include two different temperatures having precisely the same liquid density, and the higher-temperature spectrum is found to be red-shifted with respect to the lower-temperature one. Thus, a temperature effect at constant density is observed experimentally, meaning that the density-dependent explanation proffered by Nicolas *et al.*[236] cannot be complete. However, the effect measured in ref. 234 is quite small: a 0.12 eV shift between −18.0 °C and +32.6 °C, and this may simply be beyond the accuracy limitations of these simulations.

TD-DFT calculations of e^-(aq) absorption spectra in ref. 75 and 76 used a bin width of 0.15 eV to create histograms of excitation energies that simulate the envelope of the absorption spectrum. The amount of sampling that is computationally feasible is insufficient to obtain a smooth spectral envelope when a smaller bin width is used (see Fig. S5, ESI†), yet the entire experimental temperature effect that is documented in Fig. 12a amounts to only 0.2 eV and therefore almost fits within a single bin. Note also that DFT-based *ab initio* MD simulations predict a red-shift of ≤0.15 eV between normal liquid water and high-density supercritical water,[82] whereas the experimentally observed red-shift is 0.7 eV.[240] This further speaks to the difficulty in obtaining quantitative values for *T*-dependent spectral shifts from atomistic simulations.

2.12 Excited-state lifetime

Discussion of the relaxation mechanism following s → p excitation of e^-(aq) has a long history that is recapitulated here for context. The first experiments to measure this process with femtosecond time resolution noted the appearance of two distinct time constants (τ_1 = 110 fs and τ_2 = 240 fs),[62–64] which strongly suggests that the relaxation mechanism involves some nuclear dynamics, and is not simply dielectric in nature. (The intermediate state is sometimes called the "pre-solvated" or "wet" electron.[63,64,241]) Later experiments with improved time resolution were able to detect an even shorter time constant in the relaxation dynamics, τ_0 = 30–80 fs.[65,195,196]

A schematic view of the dynamics following excitation of the ground-state hydrated electron is

$$s \xrightarrow{h\nu} p^* \xrightarrow{\tau_p} p_{rlx} \xrightarrow{\tau_{IC}} s^* \xrightarrow{\tau_s} s. \quad (11)$$

Here, p* indicates a nonequilibrated, electronically-excited p state; p_{rlx} is a "relaxed" p state; and s* is the vibrationally-hot ground state. The time constant τ_p therefore characterizes solvation on the excited (p) state whereas τ_{IC} is the internal conversion (IC) time and τ_s represents the timescale for vibrational cooling on the ground state. Note that the electron's near-infrared absorption is broad and the timescales in eqn (11) overlap, with some IC occurring in tandem with solvent dynamics on the excited state. These complications led to some controversy over the interpretation of transient absorption measurements, with estimates for τ_{IC} ranging from 50 fs to 1 ps, as reviewed in ref. 241. Ultimately, two main models for interpreting the data were put forward:[195,196] an "adiabatic" model in which the IC timescale is slow ($\tau_{IC} \sim 1$ ps), so that significant solvation dynamics occur on the p state; and a "nonadiabatic" model, in which the p $\rightarrow$ s process is so fast (perhaps $\tau_{IC} < 100$ fs) that it precludes any significant solvation on the upper state. In the latter model, the slower solvation dynamics occur on the ground state.

Excited-state trajectory calculations by Schwartz and Rossky,[52,53] performed with the cavity-forming SR pseudopotential model prior to most of the detailed experimental studies of the solvation dynamics, predicted an adiabatic mechanism with a mean excited-state lifetime of 730 fs.[52] Contemporaneous experiments by Barbara's group[242,243] initially seemed to confirm this adiabatic picture,[195,244] with excited-state lifetimes reported as 300–550 fs.[196,242,243] The kinetic modeling of these experiments has recently been reexamined, however, with the conclusion that the fitting parameters are strongly correlated and that the data are fit equally well by values of τ_{IC} ranging from 100 fs (consistent with the nonadiabatic model) to 400 fs (more consistent with the original, adiabatic interpretation).[114] The adiabatic interpretation was also challenged at the time,[69,245–247] based on other transient absorption measurements that predicted much shorter IC timescales, ranging from 50–245 fs.[245–247]

Time-resolved photoelectron spectroscopy sidesteps uncertainties associated with the broad absorption in the near-infrared, and experiments of this type in both $(H_2O)_n^-$ clusters[248,249] and in liquid microjets[250–253] present a compelling case that τ_{IC} = 50–75 fs. As such, the experimental consensus now rests with the nonadiabatic model, suggesting that IC occurs in <100 fs followed by a ground-state solvation dynamics on a timescale $\tau_s \sim 400$ fs.[250,251]

This consensus is of course in contrast to the aforementioned simulation results obtained using the SR model.[52,53] These simulations have recently been updated by Schwartz and co-workers,[112,113] who performed fewest-switches surface-hopping trajectory simulations using the TB and LGS models. Despite the fact that both models predict $\tau_{IC} \sim$ 100–300 fs, the authors decide that the TB model affords an adiabatic mechanism whereas the LGS model predicts a nonadiabatic one.[112] The basis for this assignment is the fact that the TB model predicts ground-state cooling to be complete within 300 fs (with $\tau_s \sim 130$ fs) whereas this process is much slower for the LGS model ($\tau_s \sim 450$ fs). The value of τ_s obtained from the LGS simulations is in good agreement with recent experiments,[114,250,251] although Schwartz and co-workers caution that theoretical values for the excited-state lifetime of the hydrated electron are especially sensitive to decoherence effects,[112,254] which are ignored in the fewest-switches surface-hopping procedure.[254,255]

Finally, the temperature dependence of the relaxation dynamics in eqn (11) has recently been measured,[114] with values $\tau_{IC} = 158 \pm 9$ fs and $\tau_s = 430 \pm 21$ fs at $T = 298$ K that are roughly consistent with the timescales discussed above. At $T = 318$ K, these timescales are reduced to $\tau_{IC} = 73 \pm 6$ fs and $\tau_s = 369 \pm 18$ fs.[114] Reminiscent of the temperature dependence of E_{max} (Section 2.11), the TB model predicts little or no T-dependence for the excited-state lifetime, whereas the LGS model predicts a strong temperature dependence in simulations performed at constant density.[113]

3 Discussion

It should be clear from the foregoing discussion that the non-cavity LGS model represents an outlier amongst theoretical descriptions of the hydrated electron. *Ab initio* simulations consistently predict a cavity structure, whether these simulations are based on Hartree–Fock theory,[30] DFT,[25,81–85] or MP2 theory.[31] One-electron pseudopotential models developed independently by three different research groups each predict a cavity structure as well.[41,72,73]

Regarding the one-electron models, we note that the TB[72,115] and PEWP-2 models[73] were developed using essentially the same theoretical formalism as the LGS model,[20] namely, the "static-exchange" Hartree–Fock (SE-HF) approximation.[73,115,119,120] (The SR pseudopotential is developed starting from the SE-HF approximation as well, but then additional simplifying assumptions are invoked.[40]) The SE-HF approach, also known as the Phillips–Kleinman formalism,[119] starts from a Hartree–Fock calculation on $(H_2O)^-$ using frozen molecular orbitals for H_2O, because orbital relaxation constitutes electron-water polarization and is intended to be added later, by means of a classical polarization potential. It is then possible, using well-defined procedures,[73,115,119,120] to obtain a one-electron (pseudo)potential whose ground state matches the SE-HF eigenstate asymptotically (*i.e.*, at large electron-molecule separation) and whose energy equals the one-electron SE-HF eigenvalue, $\varepsilon_{SE\text{-}HF}$. The pseudopotential is first determined in some basis-set representation and is subsequently computed on a real-space grid and fit to an analytic function for use in condensed-phase simulations. In this last step, LGS apply a smoothing procedure to the data in order to reduce the grid density that is required for the simulations.[20]

The procedure outlined above is complicated by the fact that $(H_2O)^-$ is not a bound species, so in practice the SE-HF calculation is performed in the presence of a confining potential that is flat in the molecular region but rises steeply outside of this region.[73,111,115,120] In so doing, one finds that the SE-HF eigenvalue obtained in the presence of the confining potential ($\varepsilon_{SE\text{-}HF+conf}$) is more positive than the ground-state energy obtained by solving the Schrödinger equation with a confining potential but no water molecule (ε_{conf}).[21] This implies that the potential contributed by the water molecule is net

repulsive when averaged over all of three-dimensional space, because its presence increases the energy level ($\varepsilon_{\text{SE-HF+conf}} > \varepsilon_{\text{conf}}$). However, the ground-state eigenvalue ε_{LGS} that is obtained from the fitted, analytic LGS potential is smaller than the ground-state energy of the confining potential alone.[21] To summarize,

$$\varepsilon_{\text{LGS}} < \varepsilon_{\text{conf}} < \varepsilon_{\text{SE-HF+conf}}. \quad (12)$$

This implies that the LGS pseudopotential is net attractive. Most of the differences between LGS predictions and *ab initio* quantum chemistry can be understood on this basis.

In contrast to the net-attractive behavior of the LGS pseudopotential, *ab initio* simulations reveal spontaneous cavity formation upon electron injection into neat liquid water.[31,70,83] An old question in the literature is whether the aqueous electron is "trap-seeking" or "trap-digging",[256–261] *i.e.*, does it localize into a pre-existing potential well in neat liquid water, or does it drive changes in the liquid structure that create a trap? The pre-existing traps certainly exist,[260–263] in the form of transiently-broken hydrogen bonds between water molecules. Even those pseudopotentials that are net repulsive exhibit attractive regions at the hydrogen ends of the O–H bonds.

The early-time dynamics of electron localization in water have recently been simulated using *ab initio* MD with a hybrid functional.[83] The localization dynamics can be followed by examining the time evolution of the energy level defined as

$$\varepsilon = \frac{1}{2}(\varepsilon_{\text{SOMO}} + \varepsilon_{\text{LUMO}}), \quad (13)$$

which is taken in ref. 83 to be a measure of the position of the defect level relative to the conduction band edge. The time evolution of $\varepsilon(t)$ is plotted in Fig. 13a, beginning at $t = 0$ with the introduction of an electron into neat liquid water. The electron is initially unbound, indicating the absence of any very deep pre-existing traps. Nevertheless, fluctuations within just the first 50 fs afford a bound state ($\varepsilon < 0$) that may be identified as the "pre-solvated" or "wet" electron, about which much has been written.[62–66,241,264–266] Only after about 250 fs does $\varepsilon(t)$ take a steep dive in the direction of the ground-state energy of a thermalized aqueous electron, and one may identify this behavior as indicative of a transition from an initially trap-seeking electron to one that is subsequently trap-digging, with the latter behavior driven by the mostly repulsive electron-water interaction that serves to push water molecules out of the way, creating a stable cavity.

The numerical value of $\varepsilon(t)$ obtained from this periodic DFT simulation is less straightforward to interpret as compared to $\varepsilon_{\text{SOMO}}(t)$ from a Hartree–Fock simulation. From the latter, one obtains a time-averaged value $\langle\varepsilon_{\text{SOMO}}\rangle = -2.96 \pm 0.42$ eV[30] (see Fig. 11a) that is consistent with the experimental photoelectron spectroscopy of e^-(aq), within the limitations of Koopmans' theorem. In DFT calculations, however, one must contend with self-interaction error that tends to overstabilize $\varepsilon_{\text{SOMO}}$ (Fig. 11b).[118] Furthermore, in a periodic simulation of a system with a net charge, there is an additional source of uncertainty in the form of a band alignment problem.[212–215] This is related to ongoing uncertainty regarding the position of water's valence band relative to vacuum level.[25,214,215,267,268]

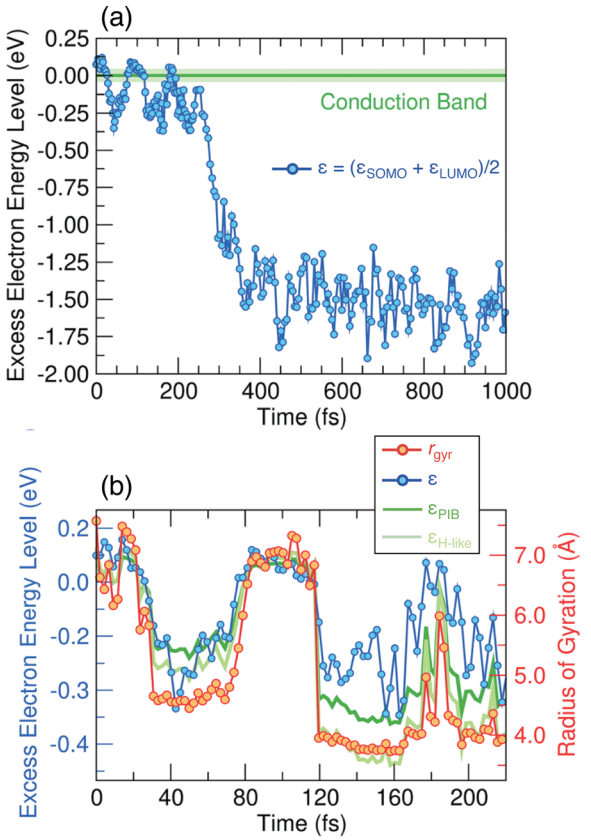

Fig. 13 (a) Energy level of an excess electron [$\varepsilon(t)$, eqn (13)] following injection into neat liquid water at $t = 0$, from an *ab initio* MD simulation using a hybrid density functional.[83] (b) Close-up view of the first 200 fs of the simulation, showing the same energy-level data along with alternative estimates of the energy level from a particle-in-a-box model (ε_{PIB}) and a hydrogen-like atom model ($\varepsilon_{\text{H-like}}$), both of which follow the $1/r_{\text{gyr}}^2$ behavior of eqn (3).[107] The quantity $r_{\text{gyr}}(t)$ is also plotted in (b) and should be read from the axis on the right. Adapted from ref. 83, published by the Royal Society of Chemistry.

What is unambiguous in the *ab initio* MD data shown in Fig. 13 is that the instantaneous energy level $\varepsilon(t)$ is strongly correlated with the radius of gyration, $r_{\text{gyr}}(t)$.[83] As discussed in Section 2.2, the instantaneous VIE and the s → p excitation energy are also strongly correlated with r_{gyr}. These correlations are observed in DFT-based simulations,[70,84,85] in periodic MP2 simulations,[31] and in simulations using cavity-forming pseudopotential models.[78,107] Similar correlations are observed in finite-size water cluster anions;[85,107] see Fig. 6.

Fig. 14 presents VIE *versus* r_{gyr} data obtained from DFT simulations by Jungwirth and co-workers,[84,85] for both $(H_2O)_n^-$ clusters as well as e^-(aq) in bulk water, which should be compared to the pseudopotential results in Fig. 6. The $1/r_{\text{gyr}}^2$ trend that arises naturally in both data sets is the analytic result for both a particle-in-a-box model and a also hydrogen-like atom model.[107] Fig. 13b plots the energy level predicted by both of these simple models alongside the *ab initio* MD data for $\varepsilon(t)$ and $r_{\text{gyr}}(t)$, demonstrating that the particle-in-a-box prediction tracks the actual DFT energy level remarkably well.

Eigenvalue data from the cavity-forming quantum chemistry simulations (either at the Hartree–Fock level, Fig. 11a, or else at

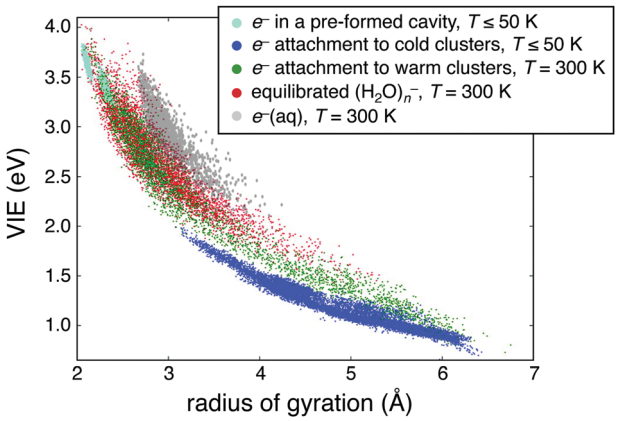

Fig. 14 VIE *versus* r_{gyr} for both $(H_2O)_n^-$ cluster anions as well as e^-(aq) in bulk water, from DFT simulations. The data shown in gray are for e^-(aq) at T = 300 K,[84] and the colored data represent clusters with various initial conditions.[85] These conditions include electron attachment to cold, neutral clusters; electron attachment to warm clusters; simulations performed in cold clusters with a pre-formed cavity; and simulations of equilibrated, anionic clusters at T = 300 K. Adapted from ref. 85 with additional data from ref. 84; copyright 2012 American Chemical Society.

the DFT level, Fig. 13) should be contrasted with what is obtained when quantum chemistry is applied after-the-fact to liquid configurations that are extracted from simulations using the LGS model. As shown in Fig. 11b, such configurations fail to bind an electron at the Hartree–Fock level, nor do they bind an electron at the PBE0 level unless a very large number of QM water molecules is included in the calculation, and then only barely.[118] In this respect, the behavior at LGS geometries is similar to what is seen at very early times in the hybrid DFT simulations of Fig. 13a, when the liquid structure still resembles neat liquid water and therefore only shallow trap states are available to accommodate an extra electron. Because the LGS pseudopotential does not expel water molecules, the SOMO eigenvalue computed with quantum chemistry is never converted to a bound state at LGS liquid geometries. In contrast, the *ab initio* electron does expel water molecules, and thereby digs its own trap, starting around t = 250 fs in Fig. 13a.

The energy-level data in Fig. 13 document the "birth" of a solvated electron starting from a delocalized conduction-band state, which might itself have arisen in water radiolysis as a secondary electron generated by ionization of water or another aqueous species by a high-energy photon or primary electron.[10] In the laboratory, solvated electrons are often generated (whether desired or not) by photoexcitation of aromatic chromophores, and *ab initio* simulations of this alternative birthing process have been reported, starting from excited states of indole[269] and phenol.[270] Subsequent thermal equilibration affords a cavity state, as shown in Fig. 1; this is the "mature" hydrated electron. To complete the life cycle, one can proceed to *ab initio* simulations of the reactivity of e^-(aq).[85,271,272] For example, in the context of what is arguably the most fundamental reaction in water radiolysis,

$$H^+(aq) + e^-(aq) \rightarrow H(aq), \qquad (14)$$

ab initio calculations suggest that the reaction is best viewed as a proton transfer reaction and not an electron-transfer reaction.[271] The same conclusion is reached based on experimental kinetics measurements.[273] The small activation barrier that is measured experimentally[208,274] is determined by the calculations to originate in the desolvation penalty needed to bring together the two ionic reactants.[271]

4 Summary and conclusions

Since 2010, Schwartz and co-workers[20,23,24,109–114] have advocated in favor of a model of e^-(aq) that does not inhabit the excluded volume that is traditionally associated with this species. While acknowledging that their alternative model is controversial, these authors contend that the controversy arises "largely because [the LGS model] does not do a good job of predicting the vertical binding energies of water anion clusters".[112] This is an apparent reference to several papers that have criticized this particular aspect of the model.[22,116,117] However, a thorough review of the known properties of e^-(aq) demonstrates that there are far more issues than this.

In fact, apart from the s → p energy gap and the (closely-related[107]) radius of gyration of the spin density, both of which are reproduced by cavity and non-cavity models alike, there are actually very few data to support the non-cavity model of e^-(aq); see Table 1. Simulations with the LGS pseudopotential do predict a strong temperature dependence for the s → p transition energy that is not seen in other models,[109] in simulations performed at constant density, although the effect is exaggerated as compared to what is observed experimentally. Once the temperature dependence of the liquid density is taken into account, however, it is no longer clear that the cavity models are qualitatively wrong,[236] although the observed effect is small and none of the simulations are in quantitative agreement with experiment. The temperature sensitivity of the LGS model manifests again in nonadiabatic trajectory simulations of the relaxation dynamics following s → p excitation. Here, the vibrational cooling timescale predicted by one of the cavity-forming models is shorter than what is observed experimentally, and also seemingly independent of temperature, whereas the LGS model qualitatively reproduces the observed temperature dependence.[113] Even so, similar excited-state lifetimes are predicted for both cavity and non-cavity models.[112]

These seem like relatively subtle issues, especially when considered in the context of challenging nonadiabatic excited-state MD simulations. They do not seem like sufficient reason to reject a structural model for e^-(aq) that successfully explains a wide variety of other observables. Simulations based on cavity-forming pseudopotential models and cavity-forming DFT calculations are in quantitative or semiquantitative agreement with experimental results from absorption spectroscopy (both λ_{max} and the higher-energy "blue tail" of the spectrum); photoelectron spectroscopy (*i.e.*, the vertical ionization energy); vibrational spectroscopy (red-shifts in the O–H stretching region of the resonance Raman spectrum, and splitting of the

bands when measured in isotopically-mixed water); and hyperfine coupling constants and *g*-factor shifts measured using EPR spectroscopy. Thermodynamic properties of e^-(aq), including its hydration energy ($\Delta_{hyd}\bar{G}^\circ$) and partial molar volume ($\bar{V}_{e^-}$), are reproduced semiquantitatively by cavity-forming DFT calculations and pseudopotential models, respectively. A careful examination of the literature, as summarized in Table 1, reveals that very few of these properties have been explained using the LGS model.

In their most recent papers,[111–114] Schwartz and co-workers have attempted to rehabilitate the image of their model by rebranding DFT-based *ab initio* MD results as predictive of a "hybrid" picture, exhibiting "only a small central cavity" and which "require significant electron-water overlap like that in our non-cavity model to reproduce experimental findings".[114] This seems, to the present author, like an attempt to carve out some narrow sense in which the LGS predictions can be considered something other than wrong. Perhaps this was inspired by the Jungwirth group's unfortunate decision to characterize their *ab initio* MD results as illustrative of the "complex nature of the hydrated electron".[84] As discussed in Section 1.1, the fact that the hydrated electron's wave function has a long tail that penetrates into the solvent has been present all along in atomistic simulations, including those performed using cavity-forming pseudopotential models.[73,87] Furthermore, there is simply no question that RDFs obtained from the cavity-forming models exhibit a sizable excluded volume into which no oxygen atoms penetrate. This is true for both one-electron models (Fig. 4a) and also many-electron *ab initio* simulations (Fig. 7). The LGS model affords no such cavity, but instead enhances the water density inside of the electron's spin density.[20] There is no "hybrid" picture.

The presence or absence of this cavity turns out to be crucial to the energy-level structure that is obtained from quantum chemistry calculations. Not only do Hartree–Fock,[30] DFT,[25,81–85] and MP2 simulations[31] all support stable cavity structures for the aqueous electron, a fact that is compelling enough in its own right, but furthermore the Hartree–Fock SOMO energy level is strongly bound in these structures, $\varepsilon_{SOMO} \approx -3.0$ eV.[30] This value is consistent, within the limitations of Koopmans' theorem, with the experimental VIE (3.7–3.8 eV).[105,106,198] A quantitative VIE of 3.75 eV is obtained from *ab initio* calculations once electron correlation and long-range polarization are included in the calculation.[79] In stark contrast, when Hartree–Fock theory is applied to liquid geometries taken from non-cavity LGS simulations, in QM/MM calculations with $\approx$75 QM water molecules, the charge-defect state is *unbound* by 0.5–1.5 eV (Fig. 11b). To entertain the LGS prediction for the structure of e^-(aq) is therefore tantamount to rejecting the notion that quantum chemistry is capable of providing even qualitatively correct energy levels.

A simpler explanation is that the LGS model is wrong. As was noted already in 2011 by Turi and Madarász,[21] the LGS model is not faithful to the static-exchange Hartree–Fock method from which it was developed. The problem appears to originate in fitting the pseudopotential data (computed on a real-space grid from *ab initio* quantum chemistry) to an analytic function for use in simulations. Unlike the TB and PEWP-2 pseudopotentials that were parameterized in much the same way,[72,73,115] the LGS pseudopotential fails to reproduce the underlying static-exchange energy level.[21] It follows from this observation that the LGS potential is net attractive, when averaged over all of three-dimensional space, whereas the underlying static-exchange Hartree–Fock approximation affords a potential that is net repulsive.[21] Most of the differences between LGS predictions and *ab initio* quantum chemistry results can be understood on this basis.

Conflicts of interest

There are no conflicts to declare.

Acknowledgements

This work was supported by National Science Foundation grant no. CHE-1665322. Isoprobability contours in Fig. 1 were obtained using a modified version of the OpenCubMan program.[275] The author thanks Francesco Ambrosio, Bhaskar Rana, and Vladimir Rybkin for providing spin densities from ref. 25, 30 and 31, respectively.

Notes and references

1 J. M. Herbert and M. P. Coons, The hydrated electron, *Annu. Rev. Phys. Chem.*, 2017, **68**, 447–472.
2 E. J. Hart, The hydrated electron, *Science*, 1964, **146**, 19–25.
3 E. J. Hart, The hydrated electron, in *Survey of Progress in Chemistry*, ed. A. F. Scott, 1969, vol. 5, pp. 129–184.
4 E. J. Hart and M. Anbar, *The Hydrated Electron*, Wiley-Interscience, 1970.
5 M. Mostafavi and I. Lampre, The solvated electron: a singular chemical species, in *Radiation Chemistry: From Basics to Applications in Material and Life Sciences*, ed. M. Spotheim-Maurizot, M. Mostafavi, J. Belloni and T. Douki, EDP Sciences, 2008, ch. 3, pp. 33–52.
6 F. S. Dainton, Recollections of the maturation of radiation chemistry, in *Early Developments in Radiation Chemistry*, ed. J. Kroh, Royal Society of Chemistry, Cambridge, UK, 1989, ch. 5, pp. 53–79.
7 J. A. LaVerne and S. M. Pimblott, Yields of hydroxyl radical and hydrated electron scavenging reactions in aqueous solutions of biological interest, *Radiat. Res.*, 1993, **135**, 16–23.
8 A. Mozumder, *Fundamentals of Radiation Chemistry*, Academic Press, San Diego, CA, 1999.
9 G. V. Buxton, An overview of the radiation chemistry of liquids, in *Radiation Chemistry: From Basics to Applications in Material and Life Sciences*, ed. M. Spotheim-Maurizot, M. Mostafavi, J. Belloni and T. Douki, EDP Sciences, 2008, ch. 1, pp. 3–16.
10 E. Alizadeh and L. Sanche, Precursors of solvated electrons in radiobiological physics and chemistry, *Chem. Rev.*, 2012, **112**, 5578–5602.

11 Y. Katsumura and H. Kudo, Radiation chemistry of aqueous solutions, in *Radiation Applications*, ed. Y. Katsumura and H. Kudo, Springer, 2018; ch. 6, vol. 7 of An Advanced Course in Nuclear Engineering, pp. 37–49.
12 Y. Gauduel, Y. Glinec and V. Malka, Femtoradical events in aqueous molecular environments: the tenuous borderline between direct and indirect radiation damages, *J. Phys.: Conf. Ser.*, 2008, **101**, 012004.
13 M. A. Huels, B. Boudaïffa, P. Cloutier, D. Hunting and L. Sanche, Single, double, and multiple double strand breaks induced in DNA by 3–100 eV electrons, *J. Am. Chem. Soc.*, 2003, **125**, 4467–4477.
14 C.-R. Wang, J. Nguyen and Q.-B. Lu, Bond breaks of nucleotides by dissociative electron transfer of non-equilibrium prehydrated electrons: a new molecular mechanism for reductive DNA damage, *J. Am. Chem. Soc.*, 2009, **131**, 11320–11322.
15 E. Alizadeh, T. M. Orlando and L. Sanche, Biomolecular damage induced by ionizing radiation: the direct and indirect effects of low-energy electrons on DNA, *Annu. Rev. Phys. Chem.*, 2015, **66**, 379–398.
16 J. Ma, S. A. Denisov, J.-L. Marignier, P. Pernot, A. Adhikary, S. Seki and M. Mostafavi, Ultrafast electron attachment and hole transfer following ionizing radiation of aqueous uridine monophosphate, *J. Phys. Chem. Lett.*, 2018, **9**, 5105–5109.
17 M. Rezaee, L. Sanche and D. J. Hunting, Cisplatin enhances the formation of DNA single- and double-strand breaks by hyrated electrons and hydroxyl radicals, *Radiat. Res.*, 2013, **179**, 323–331.
18 K. Westphal, J. Wiczk, J. Miloch, G. Kciuk, K. Bobrowski and J. Rak, Irreversible electron attachment—a key to DNA damage by solvated electrons in aqueous solution, *Org. Biomol. Chem.*, 2015, **13**, 10362–10369.
19 G. V. Buxton, C. L. Greenstock, W. P. Helman and A. B. Ross, Critical review of rate constants for reactions of hydrated electrons, hydrogen atoms and hydroxyl radicals ($^{\bullet}$OH/$^{\bullet}$O) in aqueous solution, *J. Phys. Chem. Ref. Data*, 1988, **17**, 513–886.
20 R. E. Larsen, W. J. Glover and B. J. Schwartz, Does the hydrated electron occupy a cavity?, *Science*, 2010, **329**, 65–69.
21 L. Turi and A. Madarász, Comment on ''Does the hydrated electron occupy a cavity?'', *Science*, 2011, **331**, 1387.
22 L. D. Jacobson and J. M. Herbert, Comment on ''Does the hydrated electron occupy a cavity?'', *Science*, 2011, **331**, 1387.
23 R. E. Larsen, W. J. Glover and B. J. Schwartz, Response to comment on ''Does the hydrated electron occupy a cavity?'', *Science*, 2011, **331**, 1387.
24 J. R. Casey, A. Kahros and B. J. Schwartz, To be or not to be in a cavity: the hydrated electron dilemma, *J. Phys. Chem. B*, 2013, **117**, 14173–14182.
25 F. Ambrosio, G. Miceli and A. Pasquarello, Electronic levels of excess electrons in liquid water, *J. Phys. Chem. Lett.*, 2017, **8**, 2055–2059.
26 L. Kevan, Electron spin echo studies of solvation structure, *J. Phys. Chem.*, 1981, **85**, 1628–1636.
27 L. Kevan, Solvated electron structure in glassy matrices, *Acc. Chem. Res.*, 1981, **14**, 138–145.
28 L. Kevan, Geometrical structure of solvated electrons, *Radiat. Phys. Chem.*, 1981, **17**, 413–423.
29 M. J. Tauber and R. A. Mathies, Structure of the aqueous solvated electron from resonance Raman spectroscopy: lessons from isotopic mixtures, *J. Am. Chem. Soc.*, 2003, **125**, 1394–1402.
30 Z. C. Holden, B. Rana and J. M. Herbert, Analytic energy gradients for the QM/MM-Ewald method using atomic charges derived from the electrostatic potential: theory, implementation, and application to *ab initio* molecular dynamics of the aqueous electron, *J. Chem. Phys.*, 2019, **150**, 144115.
31 J. Wilhelm, J. VandeVondele and V. V. Rybkin, Dynamics of the bulk hydrated electron from many-body wave-function theory, *Angew. Chem., Int. Ed.*, 2019, **58**, 3890–3893.
32 J. Jortner, Addendum: a conjecture on electron binding in aqueous solution, *Radiat. Res., Suppl.*, 1964, **4**, 24–34.
33 J. Jortner and S. A. Rice, Theoretical studies of solvated electrons, in *Solvated Electron*, ed. R. F. Gould, American Chemical Society Publications, Washington, D.C., 1965, ch. 2, vol. 50 of Advances in Chemistry, pp. 7–26.
34 J. Jortner and R. M. Noyes, Some thermodynamic properties of the hydrated electron, *J. Phys. Chem.*, 1966, **70**, 770–774.
35 D. A. Copeland, N. R. Kestner and J. Jortner, Excess electrons in polar solvents, *J. Chem. Phys.*, 1970, **53**, 1189–1216.
36 N. R. Kestner and J. Jortner, Radiative processes of the solvated electron in polar fluids, *J. Phys. Chem.*, 1973, **77**, 1040–1050.
37 D.-F. Feng and L. Kevan, Theoretical models for solvated electrons, *Chem. Rev.*, 1980, **80**, 1–20.
38 M. C. R. Symons, Solvated electrons or solvated solvent anions?, *Radiat. Phys. Chem.*, 1981, **17**, 425–429.
39 P. J. Rossky, J. Schnitker and R. A. Kuharski, Quantum simulation of aqueous systems, *J. Stat. Phys.*, 1986, **43**, 949–965.
40 J. Schnitker and P. J. Rossky, An electron-water pseudopotential for condensed phase simulations, *J. Chem. Phys.*, 1987, **86**, 3462–3470.
41 J. Schnitker and P. J. Rossky, Quantum simulation study of the hydrated electron, *J. Chem. Phys.*, 1987, **86**, 3471–3485.
42 P. J. Rossky and J. Schnitker, The hydrated electron: quantum simulation of structure, spectroscopy, and dynamics, *J. Phys. Chem.*, 1988, **92**, 4277–4285.
43 J. Schnitker, K. Motakabbir, P. J. Rossky and R. A. Friesner, *A priori* calculation of the optical absorption spectrum of the hydrated electron, *Phys. Rev. Lett.*, 1988, **60**, 456–459.
44 J. Schnitker and P. J. Rossky, Excess electron migration in liquid water, *J. Phys. Chem.*, 1989, **93**, 6965–6969.
45 K. A. Motakabbir and P. J. Rossky, On the nature of pre-existing states for an excess electron in water, *Chem. Phys.*, 1989, **129**, 253–262.
46 K. A. Motakabbir, J. Schnitker and P. J. Rossky, Transient photophysical hole-burning spectroscopy of the hydrated electron: a quantum dynamical simulation, *J. Chem. Phys.*, 1989, **90**, 6916–6924.

47 K. A. Motakabbir, J. Schnitker and P. J. Rossky, A comparison of classical and quantum analyses of electron localization sites in liquid water, *J. Chem. Phys.*, 1992, **97**, 2055–2060.
48 G. S. Del Buono, P. J. Rossky and T. H. Murphrey, Diffusive transport of the hydrated electron: a pseudoclassical model, *J. Phys. Chem.*, 1992, **96**, 7761–7769.
49 T. H. Murphrey and P. J. Rossky, The role of solvent intramolecular modes in excess electron solvation dynamics, *J. Chem. Phys.*, 1993, **99**, 515–522.
50 E. Keszei, S. Nagy, T. H. Murphrey and P. J. Rossky, Kinetic analysis of computer experiments on electron hydration dynamics, *J. Chem. Phys.*, 1993, **99**, 2004–2011.
51 S. J. Rosenthal, B. J. Schwartz and P. J. Rossky, Calculated photon echo signals for the aqueous solvated electron. The origin of ultrafast electronic dephasing, *Chem. Phys. Lett.*, 1994, **229**, 443–448.
52 B. J. Schwartz and P. J. Rossky, Aqueous solvation dynamics with a quantum mechanical solute: computer simulation studies of the photoexcited hydrated electron, *J. Chem. Phys.*, 1994, **101**, 6902–6916.
53 B. J. Schwartz and P. J. Rossky, Pump-probe spectroscopy of the hydrated electron: a quantum molecular dynamics simulation, *J. Chem. Phys.*, 1994, **101**, 6917–6926.
54 B. J. Schwartz and P. J. Rossky, Dynamical elements of transient spectral hole burning of the hydrated electron, *J. Phys. Chem.*, 1994, **98**, 4489–4492.
55 B. J. Schwartz and P. J. Rossky, Hydrated electrons as a probe of local anisotropy: simulations of ultrafast polarization-dependent spectral hole burning, *Phys. Rev. Lett.*, 1994, **72**, 3282–3285.
56 B. J. Schwartz and P. J. Rossky, An exploration of the relationship between solvation dynamics and spectrally determined solvent response functions by computer simulation, *J. Phys. Chem.*, 1995, **99**, 2953–2958.
57 E. Keszei, T. H. Murphrey and P. J. Rossky, Electron hydration dynamics: simulation results compared to pump and probe experiments, *J. Phys. Chem.*, 1995, **99**, 22–28.
58 B. J. Schwartz and P. J. Rossky, The isotope effect in solvation dynamics and nonadiabatic relaxation: a quantum simulation study of the photoexcited solvated electron in D_2O, *J. Chem. Phys.*, 1996, **105**, 6997–7010.
59 A. A. Mosyak, O. V. Prezhdo and P. J. Rossky, Solvation dynamics of an excess electron in methanol and water, *J. Chem. Phys.*, 1998, **109**, 6390–6395.
60 C.-Y. Yang, K. F. Wong, M. S. Skaf and P. J. Rossky, Instantaneous normal mode analysis of hydrated electron solvation dynamics, *J. Chem. Phys.*, 2001, **114**, 3598–3611.
61 J. M. Wiesenfeld and E. P. Ippen, Dynamics of electron solvation in liquid water, *Chem. Phys. Lett.*, 1980, **73**, 47–50.
62 A. Migus, Y. Gauduel, J. L. Martin and A. Antonetti, Excess electrons in liquid water: first evidence of a prehydrated state with femtosecond lifetime, *Phys. Rev. Lett.*, 1987, **58**, 1559–1562.
63 F. H. Long, H. Lu and K. B. Eisenthal, Femtosecond studies of the presolvated electron: an excited state of the solvated electron?, *Phys. Rev. Lett.*, 1990, **64**, 1469–1472.
64 H. Lu, F. H. Long and K. B. Eisenthal, Femtosecond studies of electrons in liquids, *J. Opt. Soc. Am. B*, 1990, **7**, 1511–1520.
65 R. Laenen, T. Roth and A. Laubereau, Novel precursors of solvated electrons in water: evidence for a charge transfer process, *Phys. Rev. Lett.*, 2000, **85**, 50–53.
66 P. Kambhampati, D. H. Son, T. W. Kee and P. F. Barbara, Solvation dynamics of the hydrated electron depends on its initial degree of electron delocalization, *J. Phys. Chem. A*, 2002, **106**, 2374–2378.
67 A. Hertwig, H. Hippler, A. N. Unterreiner and P. Vöhringer, Ultrafast relaxation dynamics of solvated electrons in water, *Ber. Bunsen-Ges.*, 1998, **102**, 805–810.
68 A. Hertwig, H. Hippler and A.-N. Unterreiner, Transient spectra, formation, and geminate recombination of solvated electrons in pure water UV-photolysis: an alternative view, *Phys. Chem. Chem. Phys.*, 1999, **1**, 5633–5642.
69 A. Hertwig, H. Hippler and A.-N. Unterreiner, Temperature-dependent studies of solvated electrons in liquid water with two and three femtosecond pulse sequences, *Phys. Chem. Chem. Phys.*, 2002, **4**, 4412–4419.
70 J. Savolainen, F. Uhlig, S. Ahmed, P. Hamm and P. Jungwirth, Direct observation of the collapse of the delocalized excess electron in water, *Nat. Chem.*, 2014, **6**, 697–701.
71 J. Stähler, J.-C. Deinert, D. Wegkamp, S. Hagen and M. Wolf, Real-time measurement of the vertical binding energy during the birth of a solvated electron, *J. Am. Chem. Soc.*, 2015, **137**, 3520–3524.
72 L. Turi and D. Borgis, Analytical investigations of an electron-water molecule pseudopotential. II. Development of a new pair potential and molecular dynamics simulations, *J. Chem. Phys.*, 2002, **117**, 6186–6195.
73 L. D. Jacobson and J. M. Herbert, A one-electron model for the aqueous electron that includes many-body electron-water polarization: bulk equilibrium structure, vertical electron binding energy, and optical absorption spectrum, *J. Chem. Phys.*, 2010, **133**, 154506.
74 L. Turi and P. J. Rossky, Theoretical studies of spectroscopy and dynamics of hydrated electrons, *Chem. Rev.*, 2012, **112**, 5641–5674.
75 L. D. Jacobson and J. M. Herbert, Polarization-bound quasi-continuum states are responsible for the 'blue tail' in the optical absorption spectrum of the aqueous electron, *J. Am. Chem. Soc.*, 2010, **132**, 10000–10002.
76 J. M. Herbert and L. D. Jacobson, Structure of the aqueous electron: assessment of one-electron pseudopotential models in comparison to experimental data and time-dependent density functional theory, *J. Phys. Chem. A*, 2011, **115**, 14470–14483.
77 F. Uhlig, J. M. Herbert, M. P. Coons and P. Jungwirth, Optical spectroscopy of the bulk and interfacial hydrated electron from ab initio calculations, *J. Phys. Chem. A*, 2014, **118**, 7507–7515.
78 M. P. Coons, Z.-Q. You and J. M. Herbert, The hydrated electron at the surface of neat liquid water appears to be indistinguishable from the bulk species, *J. Am. Chem. Soc.*, 2016, **138**, 10879–10886.

79 M. P. Coons and J. M. Herbert, Quantum chemistry in arbitrary dielectric environments: theory and implementation of nonequilibrium Poisson boundary conditions and application to compute vertical ionization energies at the air/water interface, *J. Chem. Phys.*, 2018, **148**, 222834.
80 A. Kumar, J. A. Walker, D. M. Bartels and M. D. Sevilla, A simple ab initio model for the hydrated electron that matches experiment, *J. Phys. Chem. A*, 2015, **119**, 9148–9159.
81 M. Boero, M. Parrinello, K. Terakura, T. Ikeshoji and C. C. Liew, First-principles molecular-dynamics simulations of a hydrated electron in normal and supercritical water, *Phys. Rev. Lett.*, 2003, **90**, 226403.
82 M. Boero, Excess electron in water at different thermodynamic conditions, *J. Phys. Chem. A*, 2007, **111**, 12248–12256.
83 M. Pizzochero, F. Ambrosio and A. Pasquarello, Picture of the wet electron: a localized transient state in liquid water, *Chem. Sci.*, 2019, **10**, 7442–7448.
84 F. Uhlig, O. Marsalek and P. Jungwirth, Unraveling the complex nature of the hydrated electron, *J. Phys. Chem. Lett.*, 2012, **3**, 3071–3075, Erratum, *ibid*. 2013, 4, 603.
85 O. Marsalek, F. Uhlig, J. VandeVondele and P. Jungwirth, Structure, dynamics, and reactivity of hydrated electrons by ab initio molecular dynamics, *Acc. Chem. Res.*, 2012, **45**, 23–32.
86 C. F. Williams and J. M. Herbert, Influence of structure on electron correlation effects and electron-water dispersion interactions in anionic water clusters, *J. Phys. Chem. A*, 2008, **112**, 6171–6178.
87 J. M. Herbert and L. D. Jacobson, Nature's most squishy ion: the important role of solvent polarization in the description of the hydrated electron, *Int. Rev. Phys. Chem.*, 2011, **30**, 1–48.
88 J. M. Herbert, The quantum chemistry of loosely bound electrons, in *Reviews in Computational Chemistry*, ed. A. L. Parill and K. Lipkowitz, Wiley-VCH, 2015, ch. 8, vol. 28, pp. 391–517.
89 I. A. Shkrob, The structure of the hydrated electron. Part 1. Magnetic resonance of internally trapping water anions: a density functional theory study, *J. Phys. Chem. A*, 2007, **111**, 5223–5231.
90 I. A. Shkrob, W. J. Glover, R. E. Larsen and B. J. Schwartz, The structure of the hydrated electron. Part 2. A mixed quantum classical molecular dynamics embedded cluster density functional theory: single-excitation configuration interaction study, *J. Phys. Chem. A*, 2007, **111**, 5232–5243.
91 M. D. Newton, Role of ab initio calculations in elucidating properties of hydrated and ammoniated electrons, *J. Phys. Chem.*, 1975, **79**, 2795–2808.
92 J. O. Noell and K. Morokuma, The hydrated electron as studied by the fractional charge MO model, *J. Phys. Chem.*, 1977, **81**, 2295–2300.
93 B. K. Rao and N. R. Kestner, *Ab initio* calculations on negatively charged water clusters, *J. Chem. Phys.*, 1984, **80**, 1587–1592.
94 T. Clark and G. Illing, Ab initio localized electron calculations on solvated electron structures, *J. Am. Chem. Soc.*, 1987, **109**, 1013–1020.
95 H. Shiraishi, K. Ishigure and K. Morokuma, An ESR study on solvated electrons in water and alcohols: difference in the *g* factor and related analysis of the electronic state by MO calculation, *J. Chem. Phys.*, 1988, **88**, 4637–4649.
96 S. Golden and T. R. Tuttle, Jr., Nature of solvated electron absorption spectra, *J. Chem. Soc., Faraday Trans. 2*, 1979, **75**, 474–484.
97 T. R. Tuttle, Jr. and S. Golden, Solvated electrons: What is solvated?, *J. Phys. Chem.*, 1991, **95**, 5725–5736.
98 D. M. Bartels, K. Takahashi, J. A. Cline, T. W. Marin and C. D. Jonah, Pulse radiolysis of supercritical water. 3. Spectrum and thermodynamics of the hydrated electron, *J. Phys. Chem. A*, 2005, **109**, 1299–1307.
99 J. V. Coe, S. M. Williams and K. H. Bowen, Photoelectron spectra of hydrated electron clusters vs. cluster size, *Int. Rev. Phys. Chem.*, 2008, **27**, 27–51.
100 A. T. Shreve, T. A. Yen and D. M. Neumark, Photoelectron spectroscopy of hydrated electrons, *Chem. Phys. Lett.*, 2010, **493**, 216–219.
101 Y. Tang, H. Shen, K. Sekiguchi, N. Kurahashi, T. Mizuno, Y. I. Suzuki and T. Suzuki, Direct measurement of vertical binding energy of a hydrated electron, *Phys. Chem. Chem. Phys.*, 2010, **12**, 3653–3655.
102 K. R. Siefermann, Y. Liu, E. Lugovoy, O. Link, M. Faubel, U. Buck, B. Winter and B. Abel, Binding energies, lifetimes and implications of bulk and interface solvated electrons in water, *Nat. Chem.*, 2010, **2**, 274–279.
103 A. Lübcke, F. Buchner, N. Heine, I. V. Hertel and T. Schultz, Time-resolved photoelectron spectroscopy of solvated electrons in aqueous NaI solution, *Phys. Chem. Chem. Phys.*, 2010, **12**, 14629–14634.
104 Y. Yamamoto, S. Karashima, S. Adachi and T. Suzuki, Wavelength dependence of UV photoemission from solvated electrons in bulk water, methanol, and ethanol, *J. Phys. Chem. A*, 2016, **120**, 1153–1159.
105 D. Luckhaus, Y. Yamamoto, T. Suzuki and R. Signorell, Genuine binding energy of the hydrated electron, *Sci. Adv.*, 2017, **3**, e1603224.
106 J. Nishitani, Y. Yamamoto, C. W. West, S. Karashima and T. Suzuki, Binding energy of solvated electrons and retrieval of true UV photoelectron spectra of liquids, *Sci. Adv.*, 2019, **5**, eaaw6896.
107 L. D. Jacobson and J. M. Herbert, Theoretical characterization of four distinct isomer types in hydrated-electron clusters, and proposed assignments for photoelectron spectra of water cluster anions, *J. Am. Chem. Soc.*, 2011, **133**, 19889–19899.
108 There is a long debate in the literature (as summarized in ref. 276) regarding whether the hydrated electron's absorption spectrum is homogeneously or inhomogeneously broadened. Briefly, early simulations using the SR pseudopotential predicted that the spectral width is dominated by inhomogeneous broadening,[52,53] *i.e.*, the broadening arises from the fact that the three dipole-allowed p states are only quasi-degenerate. Attempts to separate the homogeneous and inhomogeneous contributions to the spectrum, *via* polarized transient hole-burning experiments, have yielded

ambiguous results.[276] Abramczyk and Kroh have simulated the overall spectral envelope of solvated electrons in water and other solvents,[193,194,277] using a semi-analytic model based on strong-coupling theory,[278] and these authors conclude that "inhomogeneous broadening due to the distribution of solvent environments plays a minor role".[194] However, the homogeneous broadening mechanism in that theory relies on vibronic coupling involving modes that modulate that bond-oriented O–H$\cdots$e$^-$ solvation motif. It is unclear to the present author whether this is actually any different from the mechanism implied by atomistic simulations, where small fluctuations in the positions of first-shell water molecules are primarily responsible for "heterogeneous broadening" (as the term is used here) of the absorption spectrum.

109 J. R. Casey, R. E. Larsen and B. J. Schwartz, Resonance Raman and temperature-dependent electronic absorption spectra of cavity and noncavity models of the hydrated electron, *Proc. Natl. Acad. Sci. U. S. A.*, 2013, **110**, 2712–2717.

110 J. R. Casey, B. J. Schwartz and W. J. Glover, Free energies of cavity and noncavity hydrated electrons near the instantaneous air water interface, *J. Phys. Chem. Lett.*, 2016, **7**, 3192–3198.

111 W. J. Glover and B. J. Schwartz, Short-range electron correlation stabilizes noncavity solvation of the hydrated electron, *J. Chem. Theory Comput.*, 2016, **12**, 5117–5131.

112 C.-C. Zho and B. J. Schwartz, Time-resolved photoelectron spectroscopy of the hydrated electron: comparing cavity and noncavity models to experiment, *J. Phys. Chem. B*, 2016, **120**, 12604–12614.

113 C.-C. Zho, E. P. Farr, W. J. Glover and B. J. Schwartz, Temperature dependence of the hydrated electron's excited-state relaxation. I. Simulation predictions of resonance Raman and pump-probe transient absorption spectra of cavity and non-cavity models, *J. Chem. Phys.*, 2017, **147**, 074503.

114 E. P. Farr, C.-C. Zho, J. R. Challa and B. J. Schwartz, Temperature dependence of the hydrated electron's excited-state relaxation. II. Elucidating the relaxation mechanism through ultrafast absorption and stimulated emission spectroscopy, *J. Chem. Phys.*, 2017, **147**, 074504.

115 L. Turi, M.-P. Gaigeot, N. Levy and D. Borgis, Analytical investigations of an electron-water molecule pseudopotential. I. Exact calculations on a model system, *J. Chem. Phys.*, 2001, **114**, 7805–7815.

116 L. Turi, Hydrated electrons in water clusters: inside or outside, cavity or noncavity?, *J. Chem. Theory Comput.*, 2015, **11**, 1745–1755.

117 L. Turi, On the applicability of one- and many-electron quantum chemistry models for hydrated electron clusters, *J. Chem. Phys.*, 2016, **144**, 154311.

118 S. Dasgupta, B. Rana and J. M. Herbert, *Ab initio* investigation of the resonance Raman spectrum of the hydrated electron, *J. Phys. Chem. B*, 2019, DOI: 10.1021/acs.jpcb.9b04895.

119 C. J. Smallwood, R. E. Larsen, W. J. Glover and B. J. Schwartz, A computationally efficient exact pseudopotential method. I. Analytic reformulation of the Phillips–Kleinman theory, *J. Chem. Phys.*, 2006, **125**, 074102.

120 L. D. Jacobson, C. F. Williams and J. M. Herbert, The static-exchange electron-water pseudopotential, in conjunction with a polarizable water model: a new Hamiltonian for hydrated-electron simulations, *J. Chem. Phys.*, 2009, **130**, 124115.

121 P. Ren and J. W. Ponder, Polarizable atomic multipole water model for molecular mechanics simulation, *J. Phys. Chem. B*, 2003, **107**, 5933–5947.

122 L. D. Jacobson and J. M. Herbert, A simple algorithm for determining orthogonal, self-consistent excited-state wave functions for a state-specific Hamiltonian: application to the optical spectrum of the aqueous electron, *J. Chem. Theory Comput.*, 2011, **7**, 2085–2093.

123 L. Turi, G. Hantal, P. J. Rossky and D. Borgis, Nuclear quantum effects in electronically adiabatic quantum time correlation functions: application to the absorption spectrum of a hydrated electron, *J. Chem. Phys.*, 2009, **131**, 024119.

124 Although the electron-water pseudopotentials used in the TB[72] and LGS[20] models are derived from first principles, both models (as well as the more *ad hoc* SR model)[40] include an electron-water polarization potential with an additional adjustable parameter. In all three models, this potential is essentially $V_{\mathrm{pol}}(r) = -\alpha/r^4$, where α is the isotropic polarizability of H_2O, though the models differ in how $V_{\mathrm{pol}}(r)$ is attenuated at short range. In the TB model, a cutoff parameter r_c is fit to obtain the proper ground-state energy, *i.e.*, the VIE.[72] The SR and LGS models use a one-parameter damping function with a cutoff parameter that is chosen in a more *ad hoc* way.[40]

125 R. Baer, E. Livshits and U. Salzner, Tuned range-separated hybrids in density functional theory, *Annu. Rev. Phys. Chem.*, 2010, **61**, 85–109.

126 Á. Madarász, P. J. Rossky and L. Turi, Excess electron relaxation dynamics at water air interfaces, *J. Chem. Phys.*, 2007, **126**, 234707.

127 D. M. Sagar, C. D. Bain and J. R. R. Verlet, Hydrated electrons at the water/air interface, *J. Am. Chem. Soc.*, 2010, **132**, 6917–6919.

128 I. Carmichael, Spectral moments of solvated electrons, *Chem. Phys. Lett.*, 1978, **56**, 339–342.

129 D. M. Bartels, Moment analysis of hydrated electron cluster spectra: surface or internal states?, *J. Chem. Phys.*, 2001, **115**, 4404–4405.

130 P. Ayotte and M. A. Johnson, Electronic absorption spectra of size-selected hydrated electron clusters: $(H_2O)_n^-$, n = 6–50, *J. Chem. Phys.*, 1997, **106**, 811–814.

131 Note that ref. 31 misstates the experimental value of r_{gyr} as 2.35 Å. This value is often reported as r_{gyr} = 2.45 Å (at 25 °C), from the moment analysis in ref. 96. A smaller value of r_{gyr} = 2.16 Å had been obtained in an earlier moment analysis,[128] but subsequent to that, new experimental spectra (at various temperatures) were reported by Tuttle and Golden[232] and by Jou and Freeman.[230,231] Lineshape analysis of these data affords r_{gyr} = 2.43 Å for the former and r_{gyr} = 2.45 Å for the latter,[99] at T = 298 K.

132 J. VandeVondele and M. Sprik, A molecular dynamics study of the hydroxyl radical in solution applying self-interaction-corrected density functional methods, *Phys. Chem. Chem. Phys.*, 2005, **7**, 1363–1367.

133 The specific claim put forward in ref. 111 is that short-range electron correlation, in the form of electron-water dispersion, is crucially important in determining the structure of e^-(aq), and that its inclusion in an otherwise cavity-forming pseudopotential model might cause the excluded volume to collapse. In light of this claim, it is worth noting that the "+D3" correction that is used in both HF+D3 simulations[30,118] and the BLYP(SIC)+D3 simulations[84,85] of e^-(aq) amounts to an atom–atom dispersion potential of the form $E_{\mathrm{disp}} = -\sum_{i,j}^{\mathrm{atoms}} C_{6,ij}/R_{ij}^6$. This correction accounts for water–water dispersion (albeit approximately) but not electron-water dispersion. Inclusion of the latter at the MP2 level manifestly does not cause the excluded volume to collapse.[31]

134 A. Wallqvist, D. Thirumalai and B. J. Berne, Path integral Monte Carlo study of the hydrated electron, *J. Chem. Phys.*, 1987, **86**, 6404–6418.

135 A. Wallqvist, G. Martyna and B. J. Berne, Behavior of the hydrated electron at different temperatures: structure and absorption spectrum, *J. Phys. Chem.*, 1988, **92**, 1721–1730.

136 H. F. Hameka, G. W. Robinson and C. J. Marsden, Structure of the hydrated electron, *J. Phys. Chem.*, 1987, **91**, 3150–3157.

137 M. C. R. Symons, Aquated electrons, H_2O^- anions, and OH^-/H_3O units, *J. Phys. Chem.*, 1988, **92**, 7260–7263.

138 F. Muguet, M.-P. Bassez and G. W. Robinson, Reply to the comment "Aquated electrons, H_2O^- anions, and OH^-/H_3O units", *J. Phys. Chem.*, 1988, **92**, 7262–7263.

139 J. M. Herbert and M. Head-Gordon, Charge penetration and the origin of large O–H vibrational red-shifts in hydrated-electron clusters, $(H_2O)_n^-$, *J. Am. Chem. Soc.*, 2006, **128**, 13932–13939.

140 F. F. Muguet and G. W. Robinson, Energetics and formation of the "hydrated electron" within an itinerant radical model, *AIP Conf. Proc.*, 1994, **298**, 158–170.

141 A. L. Sobolewski and W. Domcke, Hydrated hydronium: a cluster model of the solvated electron?, *Phys. Chem. Chem. Phys.*, 2002, **4**, 4–10.

142 A. L. Sobolewski and W. Domcke, Ab initio investigation of the structure and spectroscopy of hydronium-water clusters, *J. Phys. Chem. A*, 2002, **106**, 4158–4167.

143 S. Neumann, W. Eisfeld, A. Sobolewski and W. Domcke, Simulation of the resonance Raman spectrum of the hydrated electron in the hydrated-hydronium cluster model, *Phys. Chem. Chem. Phys.*, 2004, **6**, 5297–5303.

144 S. Neumann, W. Eisfeld, A. Sobolewski and W. Domcke, Simulation of resonance Raman spectra of the solvated electron in water and methanol, in *Femtochemistry VII: Fundamental Ultrafast Processes in Chemistry, Physics, and Biology*, ed. A. W. Castleman and M. L. Kimble, Elsevier, Amsterdam, 2006, pp. 154–162.

145 A. L. Sobolewski and W. Domcke, Computational studies of aqueous-phase photochemistry and the hydrated electron in finite-size clusters, *Phys. Chem. Chem. Phys.*, 2007, **9**, 3818–3829.

146 B. Abel, U. Buck, A. L. Sobolewski and W. Domcke, On the nature and signatures of the solvated electron in water, *Phys. Chem. Chem. Phys.*, 2012, **14**, 22–34.

147 M. J. Tauber and R. A. Mathies, Fluorescence and resonance Raman spectra of the aqueous solvated electron, *J. Phys. Chem. A*, 2001, **105**, 10952–10960.

148 M. J. Tauber and R. A. Mathies, Resonance Raman spectra and vibronic analysis of the aqueous solvated electron, *Chem. Phys. Lett.*, 2002, **354**, 518–526.

149 M. Mizuno and T. Tahara, Novel resonance Raman enhancement of local structure around solvated electrons in water, *J. Phys. Chem. A*, 2001, **105**, 8823–8826.

150 M. Mizuno and T. Tahara, Picosecond time-resolved resonance Raman study of the solvated electron in water, *J. Phys. Chem. A*, 2003, **107**, 2411–2421.

151 P. Ayotte, C. G. Bailey, J. Kim and M. A. Johnson, Vibrational predissociation spectroscopy of the $(H_2O)_6^-\cdot Ar_n$, $n \geq 6$, clusters, *J. Chem. Phys.*, 1998, **108**, 444–449.

152 N. I. Hammer, J. W. Shin, J. M. Headrick, E. G. Diken, J. R. Roscioli, G. H. Weddle and M. A. Johnson, How do small water clusters bind an excess electron?, *Science*, 2004, **306**, 675–679.

153 N. I. Hammer, J. R. Roscioli and M. A. Johnson, Identification of two distinct electron binding motifs in the anionic water clusters: a vibrational spectroscopic study of the $(H_2O)_6^-$ isomers, *J. Phys. Chem. A*, 2005, **109**, 7896–7901.

154 N. I. Hammer, J. R. Roscioli, M. A. Johnson, E. M. Myshakin and K. D. Jordan, Infrared spectrum and structural assignment of the water trimer anion, *J. Phys. Chem. A*, 2005, **109**, 11526–11530.

155 J. R. Roscioli, N. I. Hammer and M. A. Johnson, Infrared spectroscopy of water cluster anions $(H_2O)_{n=3-24}^-$ in the HOH bending region: persistence of the double H-bond acceptor (AA) water molecule in the excess electron binding site of the class I isomers, *J. Phys. Chem. A*, 2006, **110**, 7517–7520.

156 W. H. Thompson and J. T. Hynes, Frequency shifts in the hydrogen-bonded OH stretch in halide-water clusters. The importance of charge transfer, *J. Am. Chem. Soc.*, 2000, **122**, 6278–6286.

157 W. H. Robertson and M. A. Johnson, Molecular aspects of halide ion hydration: the cluster approach, *Annu. Rev. Phys. Chem.*, 2003, **54**, 173–213.

158 B. Auer, R. Kumar, J. R. Schmidt and J. L. Skinner, Hydrogen bonding and Raman, IR, and 2D-IR spectroscopy of dilute HOD in liquid D_2O, *Proc. Natl. Acad. Sci. U. S. A.*, 2007, **104**, 14215–14220.

159 S. A. Corcelli, C. P. Lawrence and J. L. Skinner, Combined electronic structure molecular dynamics approach for ultrafast infrared spectroscopy of dilute HOD in liquid H_2O and D_2O, *J. Chem. Phys.*, 2004, **120**, 8107–8117.

160 S. A. Corcelli and J. L. Skinner, Infrared and Raman line shapes of dilute HOD in liquid H_2O and D_2O from 10 to 90 °C, *J. Phys. Chem. A*, 2005, **109**, 6154–6165.

161 F. Li and J. L. Skinner, Infrared and Raman line shapes for ice Ih. I. Dilute HOD in H_2O and D_2O, *J. Chem. Phys.*, 2010, **132**, 204505.

162 D. W. Silverstein, N. Govind, H. J. J. van Dam and L. Jensen, Simulating one-photon absorption and resonance Raman

scattering spectra using analytical excited state energy gradients within time-dependent density functional theory, *J. Chem. Theory Comput.*, 2013, **9**, 5490–5503.
163 J. Guthmuller, Comparison of simplified sum-over-state expressions to calculation resonance Raman intensities including Franck-Condon and Herzberg-Teller effects, *J. Chem. Phys.*, 2016, **144**, 064106.
164 J. Guthmuller, Calculation of vibrational resonance Raman spectra of molecules using quantum chemistry methods, in *Molecular Spectroscopy: A Quantum Chemistry Approach*, ed. Y. Ozaki, M. J. Wójcik, and J. Popp, Wiley-VCH, 2019, ch. 17, vol. 1, pp. 497–536.
165 E. J. Heller, The semiclassical way to molecular spectroscopy, *Acc. Chem. Res.*, 1981, **14**, 368–375.
166 E. J. Heller, R. L. Sundberg and D. Tannor, Simple aspects of Raman scattering, *J. Phys. Chem.*, 1982, **86**, 1822–1833.
167 R. M. Stratt, The instantaneous normal modes of liquids, *Acc. Chem. Res.*, 1995, **28**, 201–207.
168 P. A. Narayana, M. K. Bowman, L. Kevan, V. F. Yudanov and Y. D. Tsvetkov, Electron spin echo envelope modulation of trapped radicals in disordered glassy systems: application to the molecular structure around excess electrons in γ-irradiated 10 *m* sodium hydroxide alkaline ice glass, *J. Chem. Phys.*, 1975, **63**, 3365–3371.
169 S. Schlick, P. A. Narayana and L. Kevan, ESR line shape studies of trapped electrons in γ-irradiated ^{17}O enriched 10 *m* NaOH alkaline ice glass: model for the geometrical structure of the trapped electron, *J. Chem. Phys.*, 1976, **64**, 3153–3160.
170 A. V. Astashkin, S. A. Dikanov and Y. D. Tsvetkov, Hyperfine interactions of deuterium nuclei in the nearest surroundings of trapped electrons in alkaline glass, *Chem. Phys. Lett.*, 1988, **144**, 258–264.
171 S. A. Dikanov and Y. D. Tsvetkov, *Electron Spin Echo Envelope Modulation (ESEEM) Spectroscopy*, CRC Press, Boca Raton, 1992.
172 P. N. Moorthy and J. J. Weiss, Formation of colour centres in irradiated alkaline ice, *Philos. Mag.*, 1964, **10**, 659–674.
173 J. E. Bennett, B. Mile and A. Thomas, Electron spin resonance spectra of hydrated electrons prepared by reaction of atomic sodium with ice at 77° K, *Nature*, 1964, **201**, 919–920.
174 E. C. Avery, J. R. Remko and B. Smaller, EPR detection of the hydrated electron in liquid water, *J. Chem. Phys.*, 1968, **49**, 951.
175 R. W. Fessenden and N. C. Verma, Time resolved electron spin resonance spectroscopy. III. Electron spin resonance emission from the hydrated electron. Possible evidence for reaction to the triplet state, *J. Am. Chem. Soc.*, 1976, **98**, 243–244.
176 I. A. Shkrob and M. C. Sauer, Electron-localization in liquid acetonitrile, *J. Phys. Chem. A*, 2002, **106**, 9120–9131.
177 I. A. Shkrob, Ammoniated electron as a solvent stabilized multimer radical anion, *J. Phys. Chem. A*, 2006, **110**, 3967–3976.
178 I. A. Shkrob and T. W. Marin, Electron localization and radiation chemistry of amides, *J. Phys. Chem. A*, 2012, **116**, 1746–1757.
179 K. H. Schmidt and W. L. Buck, Mobility of the hydrated electron, *Science*, 1966, **151**, 70–71.
180 K. H. Schmidt, P. Han and D. M. Bartels, Temperature dependence of solvated electron diffusion in H_2O and D_2O, *J. Phys. Chem.*, 1992, **96**, 199–206.
181 K. H. Schmidt, P. Han and D. M. Bartels, Radiolytic yields of the hydrated electron from transient conductivity: improved calculation of the hydrated electron diffusion coefficient and analysis of some diffusion-limited (e^-)aq reaction rates, *J. Phys. Chem.*, 1995, **99**, 10530–10539.
182 J. H. Wang, Self-diffusion coefficients of water, *J. Phys. Chem.*, 1965, **69**, 4412.
183 H. S. Harned and R. L. Nuttall, The diffusion coefficient of potassium chloride in dilute aqueous solution, *J. Am. Chem. Soc.*, 1947, **69**, 736–740.
184 H. S. Harned and R. L. Nuttall, The differential diffusion coefficient of potassium chloride in aqueous solution, *J. Am. Chem. Soc.*, 1949, **71**, 1460–1463.
185 C. J. D. Fell and H. P. Hutchison, Diffusion coefficients for sodium and potassium chlorides in water at elevated temperatures, *J. Chem. Eng. Data*, 1971, **16**, 427–429.
186 V. M. M. Lobo, A. C. F. Ribeiro and L. M. P. Verissimo, Diffusion coefficients in aqueous solutions of potassium chloride at high and low concentrations, *J. Mol. Liq.*, 1998, **78**, 139–149.
187 N. Agmon, The Grotthuss mechanism, *Chem. Phys. Lett.*, 1995, **244**, 456–462.
188 M. E. Tuckerman, D. Marx and M. Parrinello, The nature and transport mechanism of hydrated hydroxide ions in aqueous solution, *Nature*, 2002, **417**, 925–929.
189 M. Chen, L. Zheng, B. Santra, H.-Y. Ko, R. A. DiStasio Jr., M. L. Klein, R. Car and X. Wu, Hydroxide diffuses slower than hydronium in water because its solvated structure inhibits correlated proton transfer, *Nat. Chem.*, 2018, **10**, 413–419.
190 D. F. Coker and B. J. Berne, Quantum calculations on excess electrons in disordered media, in *Excess Electrons in Dielectric Media*, ed. C. Ferradini and J.-P. Jay-Gerin, CRC Press, Boca Raton, FL, 1991, ch. 7, pp. 211–258.
191 K. A. Tay, F.-X. Coudert and A. Boutin, Mechanism and kinetics of hydrated electron diffusion, *J. Chem. Phys.*, 2008, **129**, 054505.
192 K. A. Tay and A. Boutin, Hydrated electron diffusion: the importance of hydrogen-bond dynamics, *J. Phys. Chem. B*, 2009, **113**, 11943–11949.
193 H. Abramczyk and J. Kroh, Absorption spectrum of the solvated electron. 2. Numerical calculations of the profiles of the electron in water and methanol at 300 K, *J. Phys. Chem.*, 1991, **95**, 6155–6159.
194 H. Abramczyk and J. Kroh, Spectroscopic properties of the solvated electron in water, alcohols, amines, ethers and alkanes, *Radiat. Phys. Chem.*, 1994, **43**, 291–297.
195 C. Silva, P. K. Walhout, K. Yokoyama and P. F. Barbara, Femtosecond solvation dynamics of the hydrated electron, *Phys. Rev. Lett.*, 1998, **80**, 1086–1089.
196 K. Yokoyama, C. Silva, D. H. Son, P. K. Walhout and P. F. Barbara, Detailed investigation of the femtosecond

pump-probe spectroscopy of the hydrated electron, *J. Phys. Chem. A*, 1998, **102**, 6957–6966.

197 A. Baltuška, M. F. Emde, M. S. Pshenichnikov and D. A. Wiersma, Early-time dynamics of the photoexcited hydrated electron, *J. Phys. Chem. A*, 1999, **103**, 10065–10082.

198 The scattering-corrected distribution of electron binding energies that is reported in ref. 105 is bimodal, with a peak at 3.7 eV but a shoulder at higher binding energy. However, Bartels[279] has questioned the consistency of the post-processing of the experimental data that led to this result. In separate experiments, using a different formulation of the correction for inelastic scattering of the outgoing photoelectron, Suzuki and co-workers report a single, Gaussian distribution of electron binding energies for e^-(aq).[106] It therefore seems likely that the shoulder reported in ref. 105 is an artifact. Nevertheless, the peak in the electron binding energy distribution that is reported in ref. 105 (3.7 ± 0.1 eV) is nearly the same as that reported in ref. 106 (3.76 ± 0.05 eV), so it seems safe to report a value of 3.7–3.8 eV for the scattering-corrected or ''genuine'' VIE of e^-(aq).

199 N. Ottoson, M. Faubel, S. E. Bradforth, P. Jungwirth and B. Winter, Photoelectron spectroscopy of liquid water and aqueous solution: electron effective attenuation lengths and emission-angle anisotropy, *J. Electron Spectrosc. Relat. Phenom.*, 2010, **177**, 60–70.

200 T. E. Gartmann, L. Ban, B. L. Yoder, S. Hartweg, E. Chasovskikh and R. Signorell, Relaxation dynamics and genuine properties of the solvated electron in neutral water clusters, *J. Phys. Chem. Lett.*, 2019, **10**, 4777–4782.

201 L. Ma, K. Majer, F. Chirot and B. von Issendorff, Low temperature photoelectron spectra of water cluster anions, *J. Chem. Phys.*, 2009, **131**, 144303.

202 J. Simons, Molecular anions, *J. Phys. Chem. A*, 2008, **112**, 6401–6511.

203 O. V. Gritsenko and E. J. Baerends, The analog of Koopmans' theorem in spin-density functional theory, *J. Chem. Phys.*, 2002, **117**, 9154–9159.

204 E. J. Baerends, O. V. Gritsenko and R. van Meer, The Kohn–Sham gap, the fundamental gap and the optical gap: the physical meaning of occupied and virtual Kohn-Sham orbital energies, *Phys. Chem. Chem. Phys.*, 2013, **15**, 16408–16425.

205 F. Buchner, T. Schultz and A. Lübcke, Solvated electrons at the water-air interface: surface *versus* bulk signal in low kinetic energy photoelectron spectroscopy, *Phys. Chem. Chem. Phys.*, 2012, **14**, 5837–5842.

206 Y. Yamamoto, Y.-I. Suzuki, G. Tomasello, T. Horio, S. Karashima, R. Mitríc and T. Suzuki, Time- and angle-resolved photoemission spectroscopy of hydrated electrons near a liquid water surface, *Phys. Rev. Lett.*, 2014, **112**, 187603.

207 U. Bovensiepen, C. Gahl, J. Stähler, M. Bockstedte, M. Meyer, F. Baletto, S. Scandolo, X.-Y. Zhu, A. Rubio and M. Wolf, A dynamic landscape from femtoseconds to minutes for excess electrons at ice-metal interfaces, *J. Phys. Chem. C*, 2009, **113**, 979–988.

208 H. Shiraishi, G. R. Sunaryo and K. Ishigure, Temperature dependence of equilibrium and rate constants of reactions inducing conversion between hydrated electrons and atomic hydrogen, *J. Phys. Chem.*, 1994, **98**, 5164–5173.

209 J. A. Mejías and S. Lago, Calculation of the absolute hydration enthalpy and free energy of H^+ and OH^-, *J. Chem. Phys.*, 2000, **113**, 7306–7316.

210 P. Han and D. M. Bartels, Reevaluation of Arrhenius parameters for $H^\bullet + OH^- \rightarrow (e^-)_{aq} + H_2O$ and the enthalpy and entropy of hydrated electrons, *J. Phys. Chem.*, 1990, **94**, 7294–7299.

211 H. A. Schwarz, Enthalpy and entropy of formation of the hydrated electron, *J. Phys. Chem.*, 1991, **95**, 6697–6701.

212 F. Costanzo, M. Sulpizi, R. G. Della Valle and M. Sprik, The oxidation of tyrosine and tryptophan studied by a molecular dynamics normal hydrogen electrode, *J. Chem. Phys.*, 2011, **134**, 244508.

213 J. Cheng and M. Sprik, Alignment of electronic energy levels at electrochemical interfaces, *Phys. Chem. Chem. Phys.*, 2012, **14**, 11245–11267.

214 F. Ambrosio, G. Miceli and A. Pasquarello, Redox levels in aqueous solution: effect of van der Waals interactions and hybrid functionals, *J. Chem. Phys.*, 2015, **143**, 244508.

215 F. Ambrosio, Z. Guo and A. Pasquarello, Absolute energy levels of liquid water, *J. Phys. Chem. Lett.*, 2018, **9**, 3212–3216.

216 C.-G. Zhan and D. A. Dixon, The nature and absolute hydration free energy of the solvated electron in water, *J. Phys. Chem. B*, 2003, **107**, 4403–4417.

217 A computed value $\Delta_{hyd}\bar{G}^\circ[e^-] = -35.5$ kcal mol^{-1} is reported in ref. 216 but corrected in ref. 80 for a better choice of standard state, affording the value of −37.4 kcal mol^{-1} that is attributed to the calculations of ref. 216 in the present work.

218 I. Janik, A. Lisovskaya and D. M. Bartels, Partial molar volume of the hydrated electron, *J. Phys. Chem. Lett.*, 2019, **10**, 2220–2226.

219 C. D. Borsarelli, S. G. Bertolotti and C. M. Previtali, Thermodynamic changes associated with the formation of the hydrated electron after photoionization of inorganic anions: a time-resolved photoacoustic study, *Photochem. Photobiol. Sci.*, 2003, **2**, 791–795.

220 C. D. Borsarelli, The partial molar volumes of hydrated proton and electron determined with time-resolved photoacoustic, *J. Phys. IV*, 2005, **125**, 11–13.

221 R. R. Hentz and D. W. Brazier, γ Radiolysis of liquids at high pressures. X. The reaction H + OH^- and the partial molar volume of the hydrated electron, *J. Chem. Phys.*, 1971, **54**, 2777–2780.

222 R. R. Hentz, Farhataziz, D. J. Milner and M. Burton, γ Radiolysis of liquids at high pressures. III. Aqueous solutions of sodium bicarbonate, *J. Chem. Phys.*, 1967, **47**, 374–377.

223 R. R. Hentz, Farhataziz and D. J. Milner, γ Radiolysis of liquids at high pressures. V. Reactions of the hydrated electron with water, *J. Chem. Phys.*, 1967, **47**, 5381–5383.

224 R. R. Hentz and R. J. Knight, γ Radiolysis of liquids at high pressures. VIII. Primary yields at 8.7 kbar and reactions of the hydrated electron with H_2O and H_3O^+, *J. Chem. Phys.*, 1970, **52**, 2456–2459.

225 R. R. Hentz, Farhataziz and E. M. Hansen, Pulse radiolysis of liquids at high pressures. II. Diffusion-controlled reactions of the hydrated electron, *J. Chem. Phys.*, 1972, **56**, 4485–4488.
226 R. R. Hentz, Farhataziz and E. M. Hansen, Pulse radiolysis of liquids at high pressures. III. Hydrated-electron reactions not controlled by diffusion, *J. Chem. Phys.*, 1972, **57**, 2959–2963.
227 W. C. Gottschall and E. J. Hart, The effect of temperature on the absorption spectrum of the hydrated electron and on its bimolecular recombination reaction, *J. Phys. Chem.*, 1966, **71**, 2102–2106.
228 B. D. Michael, E. J. Hart and K. H. Schmidt, The absorption spectrum of e_{aq}^- in the temperature range −4 to 390°, *J. Phys. Chem.*, 1971, **75**, 2798–2805.
229 R. S. Dixon and V. J. Lopata, Spectrum of the solvated electron in heavy water up to 445 K, *Radiat. Phys. Chem.*, 1978, **11**, 135–137.
230 F.-Y. Jou and G. R. Freeman, Band resolution of optical spectra of solvated electrons in water, alcohols, and tetrahydrofuran, *Can. J. Chem.*, 1979, **57**, 591–597.
231 F.-Y. Jou and G. R. Freeman, Temperature and isotope effects on the shape of the optical absorption spectrum of solvated electrons in water, *J. Phys. Chem.*, 1979, **83**, 2383–2387.
232 T. R. Tuttle, Jr. and S. Golden, Shape stability of solvated-electron optical absorption bands. Part 1.—Experimental basis, *J. Chem. Soc., Faraday Trans. 2*, 1981, **77**, 873–888.
233 H. Christensen and K. Sehested, The hydrated electron and its reactions at high temperature, *J. Phys. Chem.*, 1986, **90**, 186–190.
234 Y. Du, E. Price and D. M. Bartels, Solvated electron spectrum in supercooled water and ice, *Chem. Phys. Lett.*, 2007, **438**, 234–237.
235 Y. Yan, M. Lin, Y. Katsumura, H. Fu and Y. Muroya, Solvated electrons at elevated temperatures in different alcohols: temperature and molecular structure effects, *Radiat. Phys. Chem.*, 2010, **79**, 1234–1239.
236 C. Nicolas, A. Boutin, B. Levy and D. Borgis, Molecular simulation of a hydrated electron at different thermodynamic state points, *J. Chem. Phys.*, 2003, **118**, 9689–9696.
237 G. Wu, Y. Katsumura, Y. Muroya, X. Li and Y. Terada, Hydrated electron in subcritical and supercritical water: a pulse radiolysis study, *Chem. Phys. Lett.*, 2000, **325**, 531–536.
238 R. R. Hentz, Farhataziz and E. M. Hansen, Pulse radiolysis of liquids at high pressure. I. Absorption spectrum of the hydrated electron at pressures up to 6.3 kbar, *J. Chem. Phys.*, 1971, **55**, 4974–4979.
239 F.-Y. Jou and G. R. Freeman, Shapes of optical spectra of solvated electrons. Effect of pressure, *J. Phys. Chem.*, 1977, **81**, 909–915.
240 A. Gaathon, G. Czapski and J. Jortner, Localized excess electrons in water vapor, *J. Chem. Phys.*, 1973, **58**, 2648–2650.
241 C.-R. Wang, T. Luo and Q.-B. Lu, On the lifetimes and physical nature of incompletely relaxed electrons in liquid water, *Phys. Chem. Chem. Phys.*, 2008, **10**, 4463–4470.
242 J. C. Alfano, P. K. Walhout, Y. Kimura and P. F. Barbara, Ultrafast transient absorption spectroscopy of the aqueous solvated electron, *J. Chem. Phys.*, 1993, **98**, 5996–5998.
243 Y. Kimura, J. C. Alfano, P. K. Walhout and P. F. Barbara, Ultrafast transient absorption spectroscopy of the solvated electron in water, *J. Phys. Chem.*, 1994, **98**, 3450–3458.
244 S. Borman, Theory, experiment match on hydrated electron, *Chem. Eng. News*, 1994, **72**, 35–39.
245 M. Assel, R. Laenen and A. Laubereau, Femtosecond solvation dynamics of solvated electrons in neat water, *Chem. Phys. Lett.*, 2000, **317**, 13–22.
246 A. Thaller, R. Laenen and A. Laubereau, Femtosecond spectroscopy of the hydrated electron: novel features in the infrared, *Chem. Phys. Lett.*, 2004, **398**, 459–465.
247 M. S. Pshenichnikov, A. Baltuška and D. A. Wiersma, Hydrated-electron population dynamics, *Chem. Phys. Lett.*, 2004, **389**, 171–175.
248 A. E. Bragg, J. R. R. Verlet, A. Kammrath, O. Cheshnovsky and D. M. Neumark, Hydrated electron dynamics: from clusters to bulk, *Science*, 2004, **306**, 669–671.
249 A. E. Bragg, J. R. R. Verlet, A. Kammrath, O. Cheshnovsky and D. M. Neumark, Electronic relaxation dynamics of water cluster anions, *J. Am. Chem. Soc.*, 2005, **127**, 15283–15295.
250 M. H. Elkins, H. L. Williams, A. T. Shreve and D. M. Neumark, Relaxation mechanism of the hydrated electron, *Science*, 2013, **342**, 1496–1499.
251 M. H. Elkins, H. L. Williams and D. M. Neumark, Isotope effect on hydrated electron relaxation dynamics studies with time-resolved liquid jet photoelectron spectroscopy, *J. Chem. Phys.*, 2016, **144**, 184503.
252 S. Karashima, Y. Yamamoto and T. Suzuki, Resolving nonadiabatic dynamics of hydrated electrons using ultrafast photoemission anisotropy, *Phys. Rev. Lett.*, 2016, **116**, 137601.
253 S. Karashima, Y. Yamamoto and T. Suzuki, Ultrafast internal conversion and solvation of electrons in water, methanol, and ethanol, *J. Phys. Chem. Lett.*, 2019, **10**, 4499–4504.
254 R. E. Larsen, M. J. Bedard-Hearn and B. J. Schwartz, Exploring the role of decoherence in condensed-phase nonadiabatic dynamics: a comparison of different mixed quantum classical simulation algorithms for the excited hydrated electron, *J. Phys. Chem. B*, 2006, **110**, 20055–20066.
255 J. E. Subotnik, A. Jain, B. Landry, A. Petit, W. Ouyang and N. Bellonzi, Understanding the surface hopping view of electronic transitions and decoherence, *Annu. Rev. Phys. Chem.*, 2016, **67**, 387–417.
256 D. C. Walker, Dynamics of electron localization, *J. Phys. Chem.*, 1980, **84**, 1140–1144.
257 D. Huppert, G. A. Kenney-Wallace and P. M. Rentzepis, Picosecond infrared dynamics of electron trapping in polar liquids, *J. Chem. Phys.*, 1981, **75**, 2265–2269.
258 G. A. Kenney-Wallace and C. D. Jonah, Picosecond spectroscopy and solvation clusters. The dynamics of localizing electrons in polar fluids, *J. Phys. Chem.*, 1982, **86**, 2572–2586.
259 A. Mozumder, Conjecture on electron trapping in liquid water, *Radiat. Phys. Chem.*, 1988, **32**, 287–291.
260 M. Hilczer, W. M. Bartczak and M. Sopek, Electron localization in liquid alcohols. A statistical model, *Radiat. Phys. Chem.*, 1990, **36**, 199–202.

261 W. M. Bartczak and K. Pernal, Potential traps for an excess electron in liquid water. Geometry, energy distributions and lifetime, *Comput. Chem.*, 2000, **24**, 469–482.
262 J. Schnitker, P. J. Rossky and G. A. Kenney-Wallace, Electron localization in liquid water: a computer simulation study of microscopic trapping sites, *J. Chem. Phys.*, 1986, **85**, 2986–2998.
263 D. Nordlund, H. Ogasawara, H. Bluhm, O. Takahashi, M. Odelius, M. Nagasono, L. G. M. Pettersson and A. Nilsson, Probing the electron delocalization in liquid water and ice at attosecond time scales, *Phys. Rev. Lett.*, 2007, **99**, 217406.
264 X. Shi, F. H. Long, H. Lu and K. B. Eisenthal, Femtosecond electron solvation kinetics in water, *J. Phys. Chem.*, 1996, **100**, 11903–11906.
265 H. Iglev, S. K. Kolev, H. Rossmadl, P. S. Petkov and G. N. Vayssilov, Hydrogen atom transfer from water or alcohols activated by presolvated electrons, *J. Phys. Chem. Lett.*, 2015, **6**, 986–992.
266 J. Ma, F. Wang, S. A. Denisov, A. Adhikary and M. Mostafavi, Reactivity of prehydrated electrons toward nucleobases and nucleotides in aqueous solution, *Sci. Adv.*, 2017, **3**, e1701669.
267 W. Chen, F. Ambrosio, G. Miceli and A. Pasquarello, *Ab initio* electronic structure of liquid water, *Phys. Rev. Lett.*, 2016, **117**, 186401.
268 A. P. Gaiduk, T. A. Pham, M. Govoni, F. Paesani and G. Galli, Electron affinity of liquid water, *Nat. Commun.*, 2018, **9**, 247.
269 M. Wohlgemuth, V. Bonačić-Koutecký and R. Mitrić, Time-dependent density functional theory excited state non-adiabatic dynamics combined with quantum mechanical/molecular mechanical approach: photodynamics of indole in water, *J. Chem. Phys.*, 2011, **135**, 054105.
270 I. Sandler, J. J. Nogueira and L. González, Solvent reorganization triggers photo-induced solvated electron generation in phenol, *Phys. Chem. Chem. Phys.*, 2019, **21**, 14261–14269.
271 O. Marsalek, T. Frigato, J. VandeVondele, S. E. Bradforth, B. Schmidt, C. Schütte and P. Jungwirth, Hydrogen forms in water by proton transfer to a distorted electron, *J. Phys. Chem. B*, 2010, **114**, 915–920.
272 F. Uhlig and P. Jungwirth, Embedded cluster models for reactivity of the hydrated electron, *Z. Phys. Chem.*, 2013, **227**, 1583–1593.
273 P. Han and D. M. Bartels, H/D isotope effects in water radiolysis. 4. The mechanism of $(H)_{aq} \leftrightharpoons (e^-)_{aq}$ interconversion, *J. Phys. Chem.*, 1992, **96**, 4899–4906.
274 G. C. Barker, P. Fowles, D. C. Sammon and B. Stringer, Pulse radiolytic induced transient electrical conductance in liquid solutions. Part 1. Technique and the radiolysis of water, *J. Chem. Soc., Faraday Trans.*, 1970, **66**, 1498–1508.
275 M. Haranczyk and M. Gutowski, Visualization of molecular orbitals and the related electron densities, *J. Chem. Theory Comput.*, 2008, **4**, 689–693.
276 M. C. Cavanagh, I. B. Martini and B. J. Schwartz, Revisiting the pump-probe polarized transient hole-burning of the hydrated electron: is its absorption spectrum inhomogeneously broadened?, *Chem. Phys. Lett.*, 2004, **396**, 359–366.
277 H. Abramczyk and J. Kroh, Absorption spectrum of the solvated electron in ammonia and amines, *J. Phys. Chem.*, 1991, **95**, 5749–5753.
278 H. Abramczyk, Absorption spectrum of the solvated electron. 1. Theory, *J. Phys. Chem.*, 1991, **95**, 6149–6155.
279 D. M. Bartels, Is the hydrated electron vertical detachment genuinely bimodal?, *J. Phys. Chem. Lett.*, 2019, DOI: 10.1021/acs.jpclett.9b01790.